Magnetic and Thermal Properties of $Gd(OH)_3$ †

A. T. Skjeltorp, C. A. Catanese, * H. E. Meissner, ‡ and W. P. Wolf
Yale University, Becton Center, New Haven, Connecticut 06520
(Received 29 June 1972)

Measurements of the low-temperature specific heat have shown that $Gd(OH)_3$ undergoes a cooperative transition at 0.94 ± 0.02 K. To determine the interactions giving rise to this transition, a series of accurate susceptibility and magnetic-specific-heat measurements were made at temperatures high compared to the transition, and analyzed using asymptotically exact series expansions. The susceptibility measurements were made using an audiofrequency mutual-inductance method at temperatures between 1.4 and 4.2 K and 14.7 and 20.0 K. The magnetic specific heat was determined using two different techniques. One was the conventional calorimetric method, and measurements were made at temperatures between 0.4 and 15 K. An estimate of the lattice specific heat and a comparison with calorimetric measurements of the diamagnetic isomorph $La(OH)_3$ are given. In the other method, the magnetic specific heat was determined from the field dependence of the adiabatic differential susceptibility, using the method of Casimir and du Pré (CdP). For this, a special 4.5-MHz tunnel-diode oscillator was used, together with a sensitive temperature controller and a superconducting solenoid. Measurements were made in fields up to 15 kOe at temperatures between 5 and 68 K. Using an iterative procedure, the leading terms in the susceptibility expansion were found to be $\chi_T^{\parallel} = \lambda/(T - \theta_{\parallel}^{\infty} + B_{2\parallel}/T + B_{3\parallel}/T^2 + \cdots)$ with $\lambda = 7.815 \pm 0.008$ emu K/mole, $\theta_{\parallel}^{\infty} = 0.02 \pm 0.10$ K, $B_{2\parallel} = 2.05 \pm 0.10\,\mathrm{K}^2$, and $B_{3\parallel} = -0.59 \pm 0.10\,\mathrm{K}^3$, where $\parallel$ denotes measurements parallel to the crystal c axis and the superscript ∞ denotes correction to an infinitely long sample shape. For the magnetic specific heat, the leading terms were found to be $C_M/R = C_2/T^2 + C_3/T^3 + \cdots$, with $C_2 = 4.09 \pm 0.05\,\mathrm{K}^2$ and $C_3 = -4.2 \pm 0.7\,\mathrm{K}^3$. The unusually small error in C_2 reflects the fact that the CdP method determines $C_M T^2/R$ directly, without the necessity of first correcting for the much larger lattice specific heat. To analyze for the interactions, the dominant contributions were assumed to be of the Heisenberg form $J_n \vec{S}_0 \cdot \vec{S}_n$ with J_n restricted to nearest and next-nearest neighbors plus the calculated magnetic dipole-dipole coupling summed over all neighbors. These assumptions were tested as part of the analysis and upper limits were obtained for J_3 and for possible anisotropic nondipolar interactions. The analysis was also checked against additional susceptibility measurements perpendicular to the c axis at temperatures between 1.4 and 4.2 K and magnetization measurements in fields up to 14 kOe at temperatures between 1.1 and 4.2 K. The final results gave $J_1 = 0.180 \pm 0.005$ K and $J_2 = -0.017 \pm 0.005$ K, indicating that the system should approximate to an assembly of loosely coupled antiferromagnetic chains, but the situation is complicated by the magnetic dipole interactions which are comparable in strength. To investigate the nature of the ordering, accurate susceptibility measurements were made at temperatures between 0.6 and 1.4 K again using an inductance method. The results were interpreted as characteristic of an antiferromagnet with predominantly but not exclusively nearest-neighbor interactions. The cooperative properties of such a system are difficult to calculate, and even though all the important terms in the microscopic Hamiltonian have been determined, it has not proved possible to predict the precise nature of the ordered state. A number of possible states are discussed which probably approximate to the actual ground state, but further theoretical work on this problem is called for.

I. INTRODUCTION

The detailed analysis of a cooperative magnetic system generally involves three distinct steps: identification of the appropriate *form* of the microscopic Hamiltonian; determination of the *magnitudes* of the individual terms; and finally, a *many-body calculation* of the cooperative properties. Some approximation is usually necessary at each step, but in suitably chosen systems, the uncertainty in the first two steps can be made quite small, and it is then possible to concentrate on the theoretically more interesting many-body aspect of the problem.

One series of compounds in which it should be possible to achieve this situation are certain members of the rare-earth hydroxides $R(OH)_3$. All of these have the simple structure of the light-rare-earth trichlorides with two magnetically equivalent ions per unit cell and C_{3h} point symmetry. The structure is such that first- and second-nearest neighbors are significantly closer than other neighbors and it should therefore be possible to characterize the interactions by a reasonably small number of parameters. Moreover, their lattice parameters are some 14% smaller than those of the corresponding chlorides so that one might expect cooperative effects at readily accessible tempera-

tures. A number of magnetic, thermal, and optical measurements have already been reported for several of the hydroxides[1-13] and it seems clear that this is indeed a potentially interesting series of compounds. In this, the first paper of a series,[14,15] we want to concentrate on one which should be particularly simple and amenable to detailed analysis: $Gd(OH)_3$.

The magnetic Gd^{3+} ions are quite well described in terms of an $^8S_{7/2}$ state, for which anisotropic orbital effects vanish, and one might therefore expect $Gd(OH)_3$ to approximate to a simple isotropic Heisenberg system with nearest- and next-nearest-neighbor interactions. In this paper we shall examine the complete spin Hamiltonian for $Gd(OH)_3$ in the light of recent EPR experiments on Gd^{3+} ions[9,16] and pairs in $Y(OH)_3$ and $Eu(OH)_3$[17-20] and we shall report an analysis of a series of magnetic and thermal measurements from which quite accurate values of the interaction parameters can be determined.

The results of both our analysis and the EPR measurements[18] show that the Heisenberg form is indeed a good approximation for the exchange part of the interaction between nearest and next-nearest neighbors, but we shall also find that a number of additional terms due to magnetic dipole-dipole coupling may be unexpectedly important in this system. This is a result of some unusual cancellation effects which give rise to a situation in which the cooperative properties appear to be controlled by several of the weaker interactions. $Gd(OH)_3$ is thus an excellent example of a system in which both the form and magnitude of the interactions can be determined with some certainty, but the cooperative properties present an interesting and unusually complex problem.

The problem of inferring the cooperative properties from the spin Hamiltonian appropriate to $Gd(OH)_3$ will be discussed only briefly in this paper, but we shall be able to conclude that the ordered state should approximate to an antiferromagnetic linear chain with spins perpendicular to the crystal c axis. This is in marked contrast to the isomorphic and apparently similar system $GdCl_3$, which orders ferromagnetically with spins parallel to the c axis.[21-23] The difference can be related directly to the empirically observed variation of the exchange parameters J_1 and J_2 with changes in the interionic separations,[19] but the underlying reason for the changes in the J's remains unexplained. The present work therefore provides two additional data points for any future theoretical analysis of Gd^{3+}-Gd^{3+} exchange interactions.

The analysis in this paper uses generally well known methods, involving a fit of susceptibility and specific-heat measurements to asymptotically exact series expansions. However, in order to ensure useful accuracy for the final interaction parameters it was necessary to make very careful measurements in regions of field and temperature where the theory would be adequate, and this involved special measurement techniques which are described in Sec. IV. The theory and the fitting procedure also were treated with special care and these aspects are discussed in Secs. III and VI A. A number of additional checks and a discussion of the completeness of the final solution are given in Sec. VI D.

The problem of determining the ordered state is discussed in Sec. VII and all the principal results are finally summarized in Sec. VIII. Explicit expressions for lattice sums used in the high-temperature-series expansions of the susceptibility and specific heat are given in Appendix A together with a discussion of special features in the numerical calculations. In Appendix B a brief discussion is given of the difficulties of separating magnetic and lattice specific-heat contributions to the total specific heat, and it illustrates the great advantage of using a method which determines the magnetic part directly.

II. $Gd(OH)_3$ STRUCTURE AND SAMPLES

A. Structure

The crystallographic structure of the rare-earth-hydroxide series has been the subject of both x-ray-[24-26] and neutron-diffraction studies.[27] The symmetry of the entire series, from lanthanum to ytterbium and also yttrium[28,29] is hexagonal with space group $P6_3/m(C^2_{6h})$. For the present study, only the cation point symmetry (C_{3h}) and the magnetic cation sublattice are of interest and this is shown in Fig. 1. Also given in this figure are several near-neighbor distances for $Gd(OH)_3$, and it can be seen that the nearest and next-nearest neighbors are indeed significantly closer than other neighbors. The lattice constants used for these and all other calculations are $a = 6.30$ Å and $c = 3.61$ Å, as reported by Klevtsov and Sheina,[25] in agreement with our own x-ray diffractometer measurements.[30,31]

It may be seen that the rare-earth ions form a close-packed-hexagonal structure with a relatively small c/a ratio (0.57). The magnetic ions can be thus thought of as lying on identical chains all parallel to the c axis, with the two nearest neighbors ($n = 1$) on the same chain separated from the central reference ion by a distance of $\pm c$. The six second-nearest neighbors ($n = 2$) are situated on similar chains separated from the reference chain by a distance $a/\sqrt{3}$ and displaced a distance $\frac{1}{2}c$ along the c axis. The third-nearest neighbors ($n = 3$) are situated on six chains which are arranged in a regular hexagon around the reference ion at a distance a in the plane of the central ion.

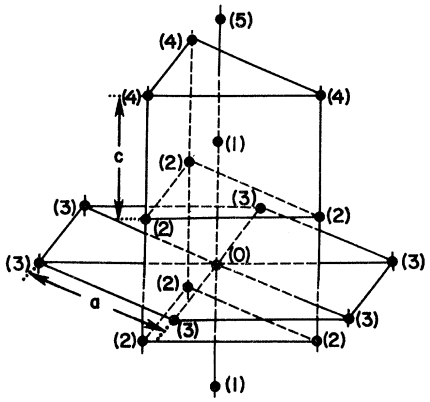

FIG. 1. Arrangement of Gd^{3+} ions in $Gd(OH)_3$. The successive neighbors and their distances from the reference ion are as follows [the distance from reference ion (Å) is in square brackets]: (0) reference ion; (1) nearest neighbor ($1n$) [3.61 ($=c$)]; (2) next-nearest neighbor ($2n$) [4.06]; (3) 3rd-nearest neighbor ($3n$) [6.30 ($=a$)]; (4) 4th-nearest neighbor ($4n$) [6.52]; (5) 5th-nearest neighbor ($5n$) [7.22]. One may note especially the relatively small distances between the nearest and next-nearest neighbors compared with the distances between other neighbors.

B. Samples

Most of the samples used for this work were small single crystals which had been prepared in this laboratory using a high-temperature (300–400 °C) high-pressure (800-atm) hydrothermal process with concentrated NaOH solution as the mineralizer. Details of the preparation are given elsewhere.[30] The crystals were generally about 1–10 mg in weight in the form of hexagonal prisms parallel to the c axis ($\sim 10\times 0.3\times 0.3$ mm) and are probably the largest and most perfect $Gd(OH)_3$ crystals made so far. Most had well-developed faces and some were quite transparent. For the specific-heat measurements much larger samples (up to 70 g) of microcrystalline powder were used, and these were prepared by a similar method but under conditions which did not favor crystallite growth.

A total of six different samples were used as described in Table I. For the samples used for the "high-temperature" magnetic measurements (I-III), it was necessary to estimate appropriate demagnetizing factors N, and this involved some uncertainty since it was not possible to shape the crystals into proper ellipsoidal forms. Moreover, for samples II and III for which more than one single crystal was used, it was necessary to minimize the effect of small air gaps between the separate pieces.[32] Fortunately, the uncertainties due to these difficulties were quite small and it was possible to estimate values of N from the corresponding values for ellipsoids of the same length to diameter ratio.[33,34] Table I gives the values for $N_{\parallel}$ corresponding to measurements parallel to the crystal axis; for measurements perpendicular to the axis we can then use the relation $N_{\parallel}+2N_{\perp}=4\pi$.

Samples I–III were aligned relative to the measuring field by eye to an accuracy of better than $\pm 3°$. The corresponding uncertainty in measuring $\chi_T^{\parallel}$ and $\chi_T^{\perp}$ was estimated to be quite negligible compared with other experimental errors.

For sample IV used for the low-temperature powder-susceptibility measurements, about 8 g of Apiezon-N grease was mixed with the hydroxide to improve the thermal conductivity and to ensure random alignment of the needle-shaped microcrystals.[35] The material was packed into a 3:1 cylinder and the demagnetizing factor was estimated using the work of Joseph.[36]

The samples used in the calorimetric measurements were made quite large so as to reduce errors due to addenda (sample holder, heater, and thermometer), and Apiezon-N grease was again used to enhance thermal equilibrium. In the earliest measurements (sample V) about 6 g of grease was mixed with 15 g of hydroxide, but in later measurements it was possible, by careful mixing, to reduce the amount of grease to 1 part in 15 while still preserving good heat contact (sample VI).

III. THEORETICAL CONSIDERATIONS

A. Effective Spin Hamiltonian

The form of the Hamiltonian for $Gd(OH)_3$ should be identical to that of other isostructural Gd^{3+} compounds, several of which have previously been studied in some detail.[37] In particular, extensive EPR experiments on Gd^{3+} in both diamagnetic trichlorides[38,39] and hydroxides [$Y(OH)_3$ and $Eu(OH)_3$[17–20]] have shown that the dominant interaction may be written in the form[40]

$$\mathcal{H}=\sum_{i>j} J_{ij}\vec{S}_i\cdot\vec{S}_j+\sum_{i>j}\alpha_{ij}[\vec{S}_i\cdot\vec{S}_j-3(\vec{S}_i\cdot\hat{r}_{ij})(\vec{S}_j\cdot\hat{r}_{ij})]$$
$$+\sum_i g\mu_B\vec{H}\cdot\vec{S}_i+V_c+H', \quad (1)$$

where $\alpha_{ij}=g^2\mu_B^2/r_{ij}^3$ is a measure of the strength of the magnetic dipole-dipole coupling and $\vec{r}_{ij}$ is the distance between ions i and j ($\hat{r}_{ij}=\vec{r}_{ij}/|\vec{r}_{ij}|$) and the effective spin $S=\frac{7}{2}$. The g factor has been found to be practically independent of the particular compound and direction, and equal to 1.992 ± 0.001.[16] We shall assume this value also for $Gd(OH)_3$ and shall show that this is in fact consistent with the measured Curie constant.

The term V_c denotes the effect of the crystal field on the $S=\frac{7}{2}$ ground state,[41] and it can be expressed in terms the usual effective spin operators O_n^m as[42]

$$V_c=\tfrac{1}{3}b_2^0O_2^0+\tfrac{1}{60}b_4^0O_4^0+\tfrac{1}{1260}(b_6^0O_6^0+b_6^6O_6^6). \quad (2)$$

TABLE I. Summary of experiments and samples.

Sample no.	Type of measurements	Temperature region (K)	Number of single crystals	Total weight	Length/ Diameter (mm)	Demagnetizing factor N[a]
I	Low-frequency susceptibility	1.4-4.2	1	2.2 mg	4/0.4	0.20 ± 0.05
	High-field magnetization	1.1-4.2				
II	Low-frequency susceptibility	14.7-20	2	30.8 mg	14/1[b]	0.15 ± 0.05
III	High-frequency susceptibility	5-68	3	18 mg	18/0.6[b]	0.10 ± 0.05
IV	Low-frequency susceptibility	0.6-1.4	polycrystalline	31 g	44/17	1.6 ± 0.1
V	Specific heat	0.4-5	polycrystalline	15 g	...	...
VI	Specific heat	2-15	polycrystalline	70 g	...	...

[a]In units in which N for a sphere is $\frac{4}{3}\pi$.

[b]Total length of the crystals laid end to end.

Spin-resonance measurements on Gd^{3+} ions in $Y(OH)_3$,[16] $La(OH)_3$,[16] and $Eu(OH)_3$[18] have shown that only the first term is appreciable, and the value of b_2^0 was found to lie in the range -0.0195 to -0.0355 K, varying slightly with temperature and the nature of the host lattice. The value appropriate to pure $Gd(OH)_3$ may be expected to lie close to this range and we therefore estimate[43] $b_2^0[Gd(OH)_3] = -0.02 \pm 0.01$ K, with a rather large error limit to allow for all the uncertainties in the interpolation. We shall see that any crystal field in this range makes only a very small contribution to the magnetic properties and the effect of the uncertainty is thus entirely negligible.

The final term in Eq. (1) represents the various higher-order interactions which have not been included explicitly. Such terms could arise from anisotropic bilinear exchange, and from electric multipole-multipole couplings via spin-orbit and crystal field admixtures into the ground state. There is good evidence from the EPR measurements[18] that all such terms are in fact very small, and we shall ignore them in the first analysis. In Sec. VI D 4 we shall make quantitative estimates of the contributions which these terms might make to the observable bulk properties and we shall show that the effects are indeed negligible.

The leading term in Eq. (1) represents the isotropic exchange coupling which generally falls off rapidly with increasing separation between the spins. From the crystal structure shown in Fig. 1 we would therefore expect the nearest-neighbor exchange constant ($J_{ij} = J_1$) and the next-nearest-neighbor constant ($J_{ij} = J_2$) to be relatively large, with all other J's very much smaller. To obtain an estimate for the upper limit of these more distant neighbor exchange interactions, we shall allow in the analysis for a possible nonzero J_3, and we shall assume that if this turns out to be small, J_4, J_5, etc., will also be small. This is reasonable not only on physical grounds, but also because the expressions for the specific heat and susceptibility contain combinations of all the J's and it would be very unlikely that several relatively large distant neighbor J's would cancel to simulate the effect of a single *small* J_3.

In contrast to the exchange interactions, the magnetic dipole interactions fall off quite slowly with distance ($\sim 1/r^3$) and we must expect comparable and cumulative effects from many neighbors. Fortunately, the dipole interaction can be estimated from the crystal structure and the g value, and there is no difficulty in calculating an arbitrary number of terms. As we shall see, most of these do in fact turn out to be quite small compared to the largest exchange interaction, but some of them may nevertheless be very important for the cooperative properties due to some interesting and complex cancellation effects. Thus, even though the dipole interaction presents no difficulty in the determination of the complete spin Hamiltonian, it does provide a challenging ingredient in the analysis of the cooperative properties of $Gd(OH)_3$.

B. High-Temperature Expansion

There is no theoretical way of estimating the three J's which were left undetermined in Eq. (1), and to obtain values from experimental data we make use of the standard method of "high-" temperature series expansion for the susceptibility and specific heat.[44–46] For this, we were able to take over some general results for systems with arbitrary symmetric tensor interactions developed by Marquard,[47,48] which he had previously applied

to the isostructural compound $GdCl_3$. The coefficients in these expansions are functions of J_1, J_2, and J_3 as well as the known dipole interactions α_{ij}, and in this section we shall give the results for the corresponding lattice sums appropriate to $Gd(OH)_3$. The final fitting of the J's to the experimental data is given in Sec. VI A.

1. Susceptibility

Because of the C_{3h} point symmetry of the hydroxides, the susceptibility χ_T is axially symmetric and can be described by $\chi_T^{\parallel}$ along the c axis and $\chi_T^{\perp}$ along any direction perpendicular to the c axis. For both directions χ_T may be expanded as a series in $1/T$ of the form[49,50]

$$\chi_T^{\alpha} = \lambda/(T - \theta_{\alpha} + B_{2\alpha}/T + B_{3\alpha}/T^2 + \cdots), \tag{3}$$

where α denotes either $\parallel$ or $\perp$. With χ_T^{α} in units of emu/mole, the Curie constant $\lambda = N_0 g^2 \mu_B^2 S(S+1)/3k_B = 7.815 \pm 0.008$ emu K/mole independent of direction, using the isotropic EPR g value 1.992 ± 0.001. We will occasionally also express χ_T^{α} in emu/cm^3 with the Curie constant $\lambda_v = \lambda/V_0$, where V_0 is the gram-atomic volume. V_0 can be calculated from the lattice constants given in Sec. II A which correspond to $V_0 = 37.4 \pm 0.4$ cm^3 and hence $\lambda_v = 0.209 \pm 0.002$ emu K/cm^3.

The first three coefficients in the denominator of Eq. (3) are found using Marquard's results to be

$$\theta = -\tfrac{21}{2}(J_1 + 3J_2 + 3J_3) + 21\Sigma'_{01}, \tag{4a}$$

$$B_2 = \tfrac{231}{4}(J_1^2 + 3J_2^2 + 3J_3^2) - \tfrac{357}{4}\Sigma'_{11} + \tfrac{903}{4}\Sigma_{02} + \tfrac{189}{2}\Sigma'_{02}, \tag{4b}$$

$$\begin{aligned} B_3 = {} & 133(J_1^3 + 3J_2^3 + 3J_3^3) - \tfrac{28665}{32}(3J_1J_2^2 + 6J_2^2J_3 + 2J_3^3) \\ & + \tfrac{1911}{64}(-120\Delta_{12} + 80\Delta_{03} + 24\Delta'_{21} - 48\Delta'_{12} + 96\Delta'_{03}) \\ & + \tfrac{133}{2}\Sigma_{30} + \tfrac{1659}{2}\Sigma_{12} - \tfrac{1883}{4}\Sigma_{03} \\ & - \tfrac{3459}{8}\Sigma'_{21} + \tfrac{4725}{8}\Sigma'_{12} - \tfrac{9471}{8}\Sigma'_{03}, \end{aligned} \tag{4c}$$

where the Σ's and the Δ's are dipolar lattice sums defined in Appendix A. All the sums except the first-order single-dipole sum Σ'_{01} in θ are independent of the external shape of the specimen. The shape dependence of θ can be treated in a simple way for ellipsoidal samples with principal axes parallel to the susceptibility axes:

$$\theta_{\alpha}(1) + N_{\alpha}(1)\lambda_v = \theta_{\alpha}(2) + N_{\alpha}(2)\lambda_v, \tag{5a}$$

where $\theta_{\alpha}(j)$ is the value for sample shape j with demagnetizing factor $N_{\alpha}(j)$. This is equivalent to the usual relation between the reciprocal susceptibilities

$$1/\chi_T^{\alpha}(1) - N_{\alpha}(1) = 1/\chi_T^{\alpha}(2) - N_{\alpha}(2). \tag{5b}$$

All measurements in this paper will be corrected to correspond to an infinite needle parallel to the c axis, for which $N_{\parallel} = 0$ and $N_{\perp} = 2\pi$, and we shall denote the corrected values of θ by $\theta_{\parallel}^{\infty}$ and $\theta_{\perp}^{\infty}$.

The evaluation of all the lattice sums was performed using the Yale IBM 7040-7094 computer and is described in Appendix A. Numerical values for the various sums appropriate to $Gd(OH)_3$ were substituted into Eqs. (4a)–(4c) and the final expressions are shown in Eqs. (6a)–(7c) below. For the susceptibility parallel to the c axis we find

$$\theta_{\parallel} = -\tfrac{21}{2}(J_1 + 3J_2 + 3J_3) + 1.441 - \lambda_v N_{\parallel} - 4b_2^0, \tag{6a}$$

$$B_{2\parallel} = \tfrac{231}{4}(J_1^2 + 3J_2^2 + 3J_3^2) - 4.690J_1 + 2.013J_2 + 1.324J_3 + 1.00, \tag{6b}$$

$$\begin{aligned} B_{3\parallel} = {} & 133(J_1^3 + 3J_2^3 + 3J_3^3) - \tfrac{28665}{32}(3J_1J_2^2 + 6J_2^2J_3 + 2J_3^3) \\ & - 18.607J_1^2 - 11.888J_1J_2 + 98.115J_2^2 \\ & - 7.175J_1J_3 - 95.655J_2J_3 - 21.895J_3^2 \\ & - 2.614J_1 - 9.304J_2 + 1.190J_3 - 0.377, \end{aligned} \tag{6c}$$

while for the susceptibility perpendicular to the c axis we obtain

$$\theta_{\perp} = -\tfrac{21}{2}(J_1 + 3J_2 + 3J_3) + 0.598 - \lambda_v(2\pi - \tfrac{1}{2}N_{\parallel}) + 2b_2^0, \tag{7a}$$

$$B_{2\perp} = \tfrac{231}{4}(J_1^2 + 3J_2^2 + 3J_3^2) + 2.345J_1 - 1.007J_2 - 0.662J_3 + 0.870, \tag{7b}$$

$$\begin{aligned} B_{3\perp} = {} & 133(J_1^3 + 3J_2^3 + 3J_3^3) - \tfrac{28665}{32}(3J_1J_2^2 + 6J_2^2J_3 + 2J_3^3) \\ & + 9.304J_1^2 + 5.944J_1J_2 - 49.058J_2^2 + 3.587J_1J_3 \\ & + 47.828J_2J_3 + 10.948J_3^2 - 6.542J_1 \\ & - 10.603J_2 + 3.936J_3 - 0.515. \end{aligned} \tag{7c}$$

In these expressions we have also included the most significant contributions of the crystal field, which may be characterized in the present case by a single parameter $b_2^0 = -0.02 \pm 0.01$ K. (See Sec. III A.) This is an unusually small value, and an order-of-magnitude estimate shows that the corresponding contributions to B_2, B_3, etc., will be entirely negligible ($<0.1\%$), and even the first-order contribution to θ is very small. In other S-state systems, higher-order crystal field contributions might well be much larger and one might also have to consider cross terms with the exchange and dipole interactions. Such effects would complicate the analysis, and even though it should be possible to allow for them we must regard the smallness of the crystal field as a very welcome simplification in the present case.

2. Magnetization

In Sec. IV A 2 we will also need an expansion for the magnetization for finite fields at relatively high temperatures. For $g\mu_B H \ll k_B T$ and $T \gg T_N$ the first approximation for M is

$$M = \frac{\lambda H}{T - \theta + B_2/T + B_3/T^2}, \tag{8}$$

in accordance with Eq. (3) for χ_T. The next-order term in the field correct to first order in the interactions can be found from the Brillouin function

$$M = Ng\mu_B S\, B_S(g\mu_B S\, H_{eff}/k_B T), \tag{9}$$

using molecular-field theory to determine the effective field

$$H_{eff} = H + AM, \tag{10}$$

where A is related to the interactions by $A = \theta/\lambda$. Combining Eq. (8) with the expansion of Eq. (9) we obtain

$$M = \frac{\lambda H}{T - \theta + B_2/T + B_3/T^2}\left(1 - \tfrac{1}{3}\alpha_S \frac{TH^2}{(T-\theta)^3}\right), \tag{11}$$

where

$$\alpha_S = \frac{1}{10}\left(\frac{g\mu_B}{k_B}\right)^2 (2S^2 + 2S + 1). \tag{12}$$

Higher-order terms in both the field and interactions could, if necessary, be found using the more general method of Van Vleck,[51,52] but it turns out that this calculation is quite complex and for the present purposes Eq. (11) will turn out to be sufficiently accurate.

3. Specific Heat

The magnetic specific heat per spin can likewise be expanded as a high-temperature series

$$C_M/R = C_2/T^2 + C_3/T^3 + \cdots. \tag{13}$$

The coefficients are generally field dependent (Sec. IV A 2), but in order to find the quantity related most directly to the interactions, we will use the zero-field value $C_M(0, T) = C_M$. In this case the coefficients in Eq. (13) are found using Marquard's results to be

$$C_2 = \tfrac{1323}{16}(J_1^2 + 3J_2^2 + 3J_3^2) + \tfrac{1323}{4}\Sigma_{02} + 21(b_2^0)^2, \tag{14a}$$

$$C_3 = \tfrac{1323}{32}(J_1^3 + 3J_2^3 + 3J_3^3) - \tfrac{83349}{32}(3J_1J_2^2 + 6J_2^2J_3 + 2J_3^3) - \tfrac{83349}{8}\Delta_{12} + \tfrac{27783}{4}\Delta_{03} - \tfrac{3969}{16}\Sigma_{12} - \tfrac{1323}{4}\Sigma_{03}. \tag{14b}$$

The term containing b_2^0 is again due to the crystal field, and using the value given in Sec. III A we can estimate the contribution to C_2 as 0.008 ± 0.008 K^2. The corresponding contribution to C_3 is estimated to be negligible.

The lattice sums Σ_{pq} and Δ_{pq} are identical to some of those for χ_T and defined in Appendix A, and substituting the values previously determined we find

$$C_2 = \tfrac{1323}{16}(J_1^2 + 3J_2^2 + 3J_3^2) + 1.348, \tag{15a}$$

$$C_3 = \tfrac{1323}{32}(J_1^3 + 3J_2^3 + 3J_3^3) - \tfrac{83349}{32}(3J_1J_2^2 + 6J_2^2J_3 + 2J_3^3) - 18.89J_1 - 35.02J_2 + 8.40J_3 - 1.29, \tag{15b}$$

where we have included in C_2 the small crystal field contribution which accounts for only about 0.2% of the total. The computer programs for both these expressions were checked by evaluating them also for the parameters appropriate to $GdCl_3$ and comparing the results against the published values.[47] As before, the agreement was perfect within the estimated accuracies.

4. Discussion

It can be seen that the expansion coefficients for both χ_T and C_M increase rather rapidly in complexity with increasing order, and that it would be quite difficult to compute any of the higher-order terms for a system such as $Gd(OH)_3$ with appreciable long-range interactions. Fortunately, the eight coefficients which we have been able to calculate are more than enough in the present case, since there are only two (or possibly three) unknown interaction parameters to be fitted. For other systems containing non S-state ions we must generally expect more complex forms for the interactions,[53,54] and the series-expansion method can then be used only if the form of the interactions can be simplified by some other considerations, such as a dominant crystal field anisotropy. We shall consider a case of this kind in the second paper of the present series,[15] in which we shall discuss $Tb(OH)_3$.

It is interesting to note one feature of the present results which illustrates a general problem which may be important in all systems with long-range interactions. This concerns the relatively large contributions from cross terms between the larger near-neighbor interactions and the many weaker far-neighbor interactions. These terms seem to become more important in the higher-order expansion coefficients and this suggests that special care must be taken to include longer-range interactions in calculating these coefficients. Physically, this may be related to the fact that as the temperature decreases and the average range of the correlations increases, the effect of direct long-range interactions on the correlation between more distant neighbors may become comparable to the higher-order effects of short-range interactions.

It is also of some interest to compare the present numerical results with the corresponding coefficients for $GdCl_3$, since this illustrates the possible sensitivity of the various sums to small changes of lattice structure. Part of any difference is of course due to a simple change of scale, since each dipole interaction is proportional to g^2/c^3. Allowing for this scale factor we then still find differences ranging from 2 to 10%, depending on the order of the dipole sum. These may be compared with the difference between the c/a ratios in the two lattices which is only about 2%. This shows that it is generally not very accurate to extrapolate lattice sums (and especially the higher-order sums) from one lattice to another, even when they are apparently quite similar.

IV. EXPERIMENTAL METHODS

A. Specific-Heat Measurements

To measure the magnetic specific heat, two different techniques were employed. One was the conventional electrical-heating method, in which one measures the total specific heat which is then analyzed to allow for the lattice contribution. The other was a magnetic high-frequency method, which determines C_M directly. As we shall see, the two methods are complementary in the present case, the first being more accurate below about 5 K, while the other is more accurate at higher temperatures.

1. Calorimetric Method

The measurement of the total specific heat was carried out in the usual way by subjecting a thermally isolated sample to a measured pulse of Joule heat and determining the change of temperature. Measurements were made from 0.4 to 15 K, using a cryostat equipped for both He^3 and He^4 cooling. A detailed description of both the calorimeter and the experimental procedure is given elsewhere,[55,56] but there were a few special features in the present experiments which require comment.

One arose from the fact that the samples were microcrystalline (Sec. II B) and this involved using a copper container and grease to promote thermal equilibrium. The heat capacity of the calorimeter plus grease was measured separately and subtracted. Below about 5 K this led to only a small uncertainty, but at higher temperatures it increased to a possible error of about 2% at 10 K. At these temperatures, this correction represented the largest error in the experiment. The uncertainty in the specific-heat measurements themselves was generally less than 1%.

A more serious uncertainty arose in the analysis to determine the magnetic part of the specific heat. This involved making an estimate of the lattice contribution, which, as we shall show in Appendix B is far less certain than is sometimes supposed. At temperatures below about 5 K the lattice correction becomes quite small (< 3% of the total) and the corresponding uncertainty in the final values of C_M is less than 0.3%. At higher temperatures, however, the correction becomes very large, and at 13 K, for example, it accounts for about 80% of the total specific heat. An estimated uncertainty of about 9% in the correction then implies a possible error of about 30% in the final value of C_M. In this region it is necessary therefore either to improve the accuracy of the lattice estimate or to devise a technique which can measure C_M directly. Fortunately, such a technique is in fact available in the form of the Casimir and du Pré method, which we shall now discuss.

2. High-Frequency Specific-Heat Measurements

The method of Casimir and du Pré[57,58] involves measuring the field dependence of the adiabatic magnetic susceptibility $\chi_S(H)$, which can then be related to C_M using simple thermodynamics and a knowledge of the static (isothermal) magnetic properties. Details of the method and apparatus using a tunnel-diode oscillator have been described in some detail previously,[6,59,60] and some recent improvements in the technique are being published elsewhere.[61]

Measurements were made between 5 and 68 K, the upper limit being set by the temperature-control system in our particular cryostat. The lower limit represents a temperature below which the uncertainty in the static terms relating $\chi_S(H)$ to C_M exceeds the error in the analysis of the total specific heat, which becomes more accurate as the lattice contribution decreases in importance. The high-frequency method is thus complementary to the usual electrical-heating method, and it is particularly useful for temperatures high compared to the cooperative transition.

A necessary condition for obtaining the appropriate adiabatic susceptibility is that the measuring frequency must be high compared to the spin-lattice relaxation rate but slow compared to the spin-spin relaxation rate. For $Gd(OH)_3$ this condition can fortunately be satisfied very easily. Due to the predominantly S-state character of the ground state, the spin-lattice relaxation rate of Gd^{3+} compounds is generally quite slow[62] ($\tau_{SL}^{-1} < 10^7$ sec^{-1} at $T \simeq 70$ K and decreasing for lower temperatures), while the spin-spin rate is typically much faster[63] ($\tau_{SS}^{-1} \sim 10^{10}$ sec^{-1}, and essentially temperature independent). A wide range of frequencies f will therefore satisfy the condition $\tau_{SL}^{-1} \ll 2\pi f \ll \tau_{SS}^{-1}$ and for convenience we chose $f = 4.5$ MHz. Under these conditions the real part of the measured differential susceptibility $\chi'(H)$ will be equal to the adiabatic susceptibility $\chi_S(H)$ of the spin system in internal equilibrium but isolated from the lattice.

The relation between the susceptibility measured under these conditions and C_M is given by[61,64]

$$\frac{C_M(H,T)}{R} = \left[T\left(\frac{\partial M}{\partial T}\right)_H^2 \Big/ R\,\chi_T(H)\right]\left(\frac{\chi'(0)\,\chi_T(H)}{\chi'(H)\,\chi_T(0)} - 1\right)^{-1}, \tag{16}$$

where $\chi_T(H) = (\partial M/\partial H)_T$ is the isothermal differential susceptibility in a field H. If the field and temperature variation of the static magnetization $M(H,T)$ is known, all the remaining terms on the right-hand side of Eq. (16) can be calculated, and in the present case this could be done to sufficient accuracy using the limited expansion, Eq. (11). The magnetic specific heat can thus be related to a *ratio* of susceptibilities $\chi'(0)/\chi'(H)$, which can be measured quite conveniently.

In general, we must of course expect $C_M(H, T)$ to be field as well as temperature dependent (Sec. III B 3), and in order to find the quantity related most directly to the interactions [Eq. (13)], $C_M(0, T)$, we can use the thermodynamic relationship[61]

$$\left(\frac{\partial C_M}{\partial M}\right)_T = -T\left(\frac{\partial^2 H}{\partial T^2}\right)_M. \tag{17}$$

This combined with Eq. (16) using M in Eq. (11) gives the magnetic specific heat in zero field,

$$\frac{C_M(0,T)T^2}{R} \simeq \frac{\lambda}{R}\left(\frac{T}{T-y}\right)^3(1-y')^2 r(H,T) \times\left(1+\alpha_S \frac{T}{(T-\theta)^3} r(H,T)\right) -\frac{1}{2}\frac{\lambda}{R}\frac{T^3 y''}{(T-y)^2}H^2, \tag{18}$$

where the last term represents the field dependence of C_M to lowest order, and where

$$r(H,T) = \frac{H^2}{\chi'(0)/\chi'(H) - 1}, \tag{19}$$

$$y = \theta_{\text{II}} - B_{2\text{II}}/T - B_{3\text{II}}/T^2, \tag{20}$$

$$y' = \frac{dy}{dT} = \frac{B_{2\text{II}}}{T^2} + \frac{2B_{3\text{II}}}{T^3}, \tag{21}$$

$$y'' = \frac{d^2y}{dT^2} = \frac{-2B_{2\text{II}}}{T^3} - \frac{6B_{3\text{II}}}{T^4}. \tag{22}$$

The constants α_S and λ/R appropriate to $Gd(OH)_3$ may be estimated from Eq. (12) and the value for λ given in connection with Eq. (3):

$$\alpha_{7/2} = 0.058\,10 \pm 0.000\,06\ (\text{K/kOe})^2$$

and

$$\lambda/R = 0.094\,00 \pm 0.000\,09\ (\text{K/kOe})^2.$$

Values for the other parameters will be estimated as discussed in Sec. VI.

The experimentally determined function $r(H, T)$ in Eq. (19) should thus be independent of H to the extent that the field dependence of C_M can be neglected, and to simplify the analysis this was ensured by limiting the maximum value of H used at each temperature. Within the limits of accuracy of the present experiments (±0.3%), this implied a maximum H of 0.3 kOe at 5 K rising to about 15 kOe at 68 K.

To check the validity of the expression for the field dependence a series of measurements at higher fields was also made at one of the lowest temperatures, and a value was obtained for the coefficient of H^2 in Eq. (18). Comparison with the calculated value provided a useful check on the parameters used in the final expression for y.

B. Low-Frequency Susceptibility Measurements

These experiments can be described conveniently in two parts: single-crystal measurements above 1.4 K and powder measurements below 1.4 K.

1. Single-Crystal Measurements

Susceptibility measurements were performed at liquid-He^4 temperatures (1.4–4.2 K) and liquid-hydrogen temperatures (14.7–20.0 K) using the method of McKim and Wolf.[65] In this method the susceptibility is determined from the change of mutual inductance of a double-coil system when the sample is moved relative to the coil, using an audio-frequency Hartshorn bridge. The apparatus was calibrated with several multicrystal samples of manganous ammonium sulphate $[Mn(NH_4)_2(SO_4)_2 \cdot 6H_2O]$. From the reproducibility of different samples we judge the absolute calibration accuracy to be about ±0.5%. The relative accuracy for the temperature dependence of χ_T for one particular sample, on the other hand, was very much better than this and was estimated to be about ±0.1%. The temperature in both the hydrogen and helium ranges was found from the vapor pressure above the coolant after correction for the hydrostatic head pressure, and the uncertainty in this (~0.1%) is probably the main contribution to the scatter in the data for any one sample.

2. Powder Measurements below 1.4 K

Measurements of the susceptibility were made from 0.6 to 1.4 K using a He^3 cryostat described elsewhere.[55] The much lower sensitivity of this system made it impossible to measure the small single crystals available, and a much larger multicrystalline sample was therefore used (see Table I, sample IV).

The susceptibility was again determined by an inductance method, but since it was now not possible to move the sample relative to the coil only changes in χ_T could be measured. However, by extending the measurements up to 4.2 K and comparing the results with the previously determined absolute single-crystal susceptibilities, it was possible to normalize the powder data to an accuracy of about 1%. Care was taken to avoid spurious contributions from the cryostat by keeping all parts at a fixed low temperature and varying only the temperature of the sample, using an electrical heater wound directly on the sample. The temperature was measured with a germanium resistor calibrated *in situ* against the vapor pressure of He^3 and He^4. In the temperature range between 0.6 and 1.4 K this calibration was estimated to be accurate to better than 0.005 K.

C. Magnetization Measurements

Measurements of the magnetization in fields up to 14 kOe at temperatures between 1.1 and 4.2 K were made using a Foner-type vibrating-sample magnetometer. Details of the apparatus are given elsewhere,[55] but we may here note the fairly high sensitivity ($\sim 2\times10^{-4}$ emu) which enabled us to measure quite small samples (See Table I, sample I) to a relative accuracy of about 0.1% at the maximum field. The absolute accuracy, which involves the calibration of the apparatus and the mass of the sample, was about 1%.

Magnetization measurements were made both parallel and perpendicular to the crystal c axis by aligning the sample in a horizontal plane and rotating the magnet. For the parallel direction, the maximum alignment error was judged to be $\pm 3°$, while for the perpendicular direction it was essentially zero. The low-field results for both directions were checked against the ac susceptibility measurements (Sec. V F) and good agreement was found.

V. EXPERIMENTAL RESULTS

A. Calorimetric Specific-Heat Measurements

The results of the calorimetric total-specific-heat measurements are shown in Fig. 2. The most striking feature is the sharp peak at 0.94 ± 0.02 K, which is clearly associated with a cooperative phase transition.[66] There is also a noticeable broad shoulder on the high-temperature side, which we shall later interpret as due to short-range order in a predominantly one-dimensional system. The nature of the phase transition will be discussed further in Sec. VII B.

At the lowest temperatures, the measured total specific heat is almost entirely due to the magnetic contributions, but at higher temperatures the lattice becomes increasingly important. In order to estimate the lattice contribution C_L, additional specific-heat measurements were made on $La(OH)_3$ between 4.2 and 15 K, and compared with measurements on $Gd(OH)_3$ over the same range. The results of this analysis are given in Appendix B, which also includes a second estimate of C_L based on a comparison of the calorimetric and high-frequency measurements on $Gd(OH)_3$. A comparison of the two estimates indicates a rather large difference which is not readily explained. For the present we must therefore set a correspondingly large uncertainty on C_L, and we conclude that $C_L/R=(3.4\pm0.3)\times10^{-5}T^3$.

Using this relation we can find C_M from the measured total, but the correction is quite small (<3%) over the range covered by Fig. 2, and the corresponding uncertainty is less than 0.3% of C_M. However, at higher temperatures the uncertainty increases rapidly, and at 13 K it accounts for a possible error of 30%. We shall therefore use the calorimetric results only below about 4 K and rely on the high-frequency data at higher temperatures.

B. High-Frequency Specific-Heat Measurements

Measurements of the relative field dependence of the adiabatic susceptibility $\chi'(H)/\chi'(0)$ were made at 21 different temperatures in the range 5–68 K, for about 13 different values of H at each temperature. The maximum field at each temperature was determined from the condition of a field independent C_M according to Eq. (18) to better than 0.3%.

The method of analysis to determine the asymptotic value of the function $r(T)=r(H\to0,T)$ from plots of $\chi'(0)/\chi'(H)-1$ vs H^2 is discussed else-

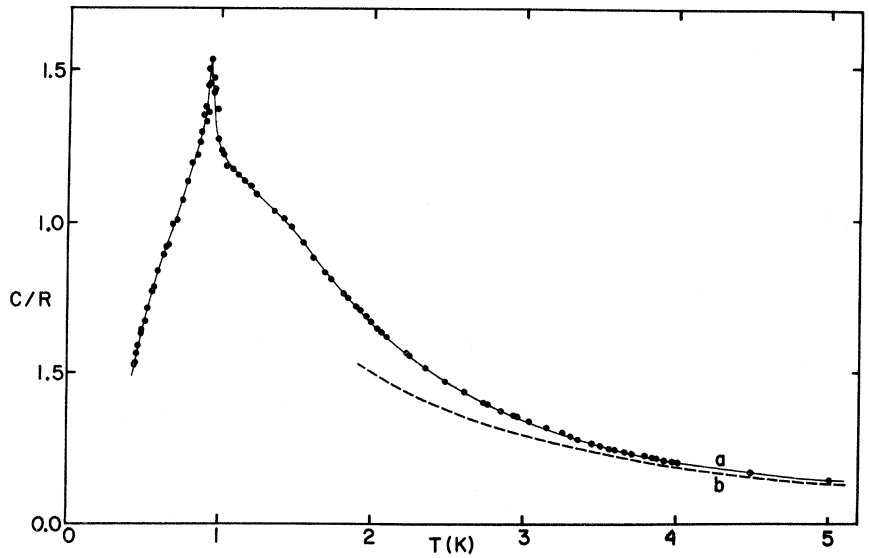

FIG. 2. Total specific heat of $Gd(OH)_3$ from calorimetric measurements, curve a, which is very close to the magnetic specific heat in that the lattice specific heat contributes a maximum of about 3% at 5 K. The peak corresponds to $T_N=0.94\pm0.02$ K and is interpreted as the onset of a complex long-range antiferromagnetic order. Curve b is the high-temperature asymptote $C_M/R=C_2/T^2+C_3/T^3$ as calculated from the final values of the interactions.

where[22] and it was generally found that $r(T)$ could be estimated to about $\pm 0.5\%$. The values were slightly less accurate for the lowest temperatures as the maximum allowed field becomes smaller with a correspondingly smaller variation in $\chi'(H)/\chi'(0)$. But even at the lowest temperature $r(T)$ could be estimated to better than $\pm 1\%$.

To find $C_M(0, T)T^2/R$ using Eq. (18) it was also necessary to estimate values for the expansion parameters $\theta_{\parallel}$, $B_{2\parallel}$, and $B_{3\parallel}$, and this was done iteratively as discussed in Sec. VI A. The values finally adopted were $\theta_{\parallel} = 0.00 \pm 0.10$ K (corrected to the shape of the high-frequency sample), $B_{2\parallel} = 2.05 \pm 0.10$ K^2, and $B_{3\parallel} = -0.59 \pm 0.10$ K^3. Substituting these values and the experimentally determined $r(T)$ in Eq. (18) we obtain the results shown in Fig. 3, in which we plot $C_M(0, T)T^2/R$ as a function of $1/T$. The error bars represent the combined uncertainties from the parameters used in the analysis as well as experimental errors in estimating $r(T)$.

It may be seen that the over-all errors are quite small, especially at the highest temperatures, which are the most important for the determination of the high-temperature asymptote. At the lowest temperatures the errors become somewhat larger, mainly due to uncertainties in the static parameters $\theta_{\parallel}$, $B_{3\parallel}$, but fortunately the calorimetric estimates of C_M become more accurate in this region. These are also shown in Fig. 3 and it can be seen that they provide an excellent complement to the high-frequency measurements.

Comparing the two sets of data in the region of overlap one may attempt to refine the values of the various correction factors which enter into the two analyses and in particular one can obtain a better value of C_L, as will be discussed in Appendix B. Using independent estimates $B_{2\parallel}$ and $B_{3\parallel}$ (see Sec. VI A), one can also use a comparison of the low-temperature data to obtain an improved value of $\theta_{\parallel}$. With the relative uncertainties in the present results no significant improvement in the estimate of $\theta_{\parallel}$ could be obtained, but in some cases this may prove to be quite a sensitive check.[67]

C. Entropy and Internal Energy of the Magnetic System

The zero-field magnetic-specific-heat measurements permit calculation of other thermodynamic functions such as the entropy $S_M(T)/R$ and the internal energy $U_M(T)/R$, which can provide useful checks of both the measurements and the analysis. Given C_M/R we have

$$S_M(T)/R = \int_0^T (C_M/RT)\,dT \tag{23}$$

and

$$U_M(T)/R = \int_{\infty}^T (C_M/R)\,dT, \tag{24}$$

where the zero of U_M has been chosen such that $U_M \to 0$ as $T \to \infty$. In practice, C_M is available over

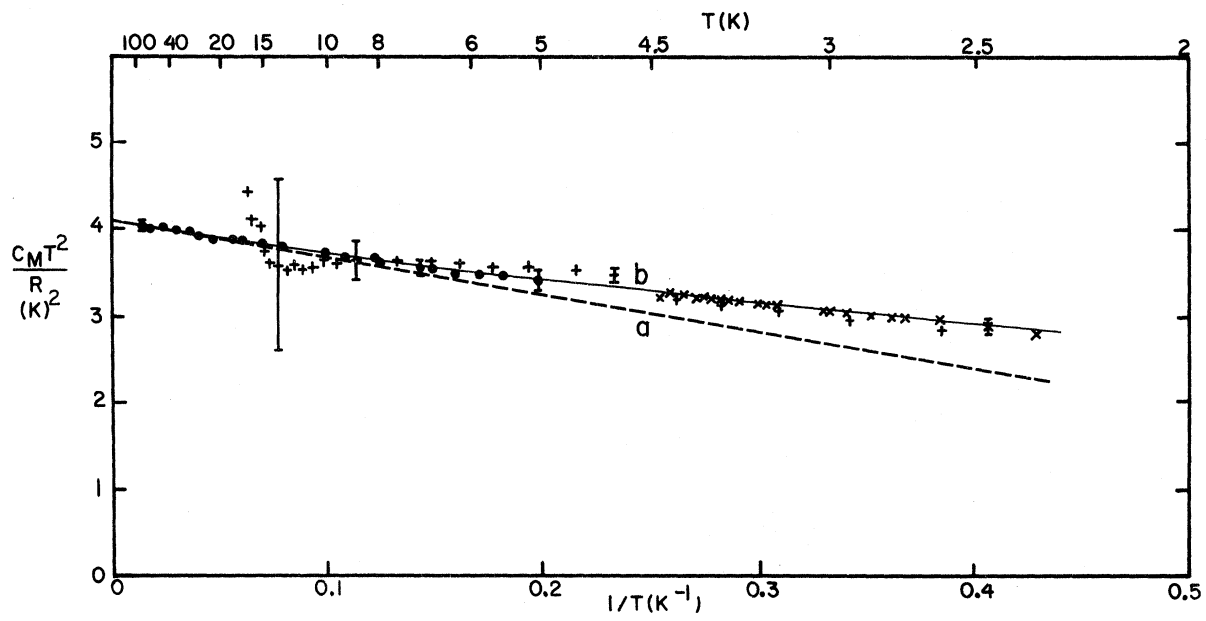

FIG. 3. High-temperature magnetic specific heat for $Gd(OH)_3$ from high-frequency susceptibility measurements (•) and calorimetric measurements on samples V (×) and VI (+), plotted as $C_M T^2/R$ vs $1/T$ to identify the first two terms in the high-temperature expansion $C_M T^2/R = C_2 + C_3/T$. The line a is the high-temperature asymptote, with $C_2 = 4.09 \pm 0.05$ K^2 and $C_3 = -4.2 \pm 0.7$ K^3. This was found from the high-frequency data using small corrections from higher-order terms in the expansion as determined from the calorimetric data. Curve b is the result of the self-consistent fitting procedure described in the text.

only a finite range of T and both low- and high-temperature extrapolations are required. In the present case, the high-temperature extrapolation presents no difficulty, since the asymptotic expansion of C_M has been determined quite accurately (see Secs. V B and VI A), but the low-temperature contribution ($T < 0.4$ K) must be estimated and this introduces a small uncertainty. Fortunately, the major contribution to both S_M and U_M comes from the region over which good measurements of C_M are available and both functions can therefore be estimated with good accuracy. Both curves have the generally expected shapes and we shall here quote only a few values which are of interest.

For the total entropy one finds

$$S_M(\infty)/R = 2.0 \pm 0.2$$

and this is in excellent agreement with the value $\ln 8 = 2.08$ expected for a system with $S = \frac{7}{2}$. This agreement provides at least a rough check on the normalization of the specific-heat measurements. For the entropy at the transition one finds

$$S_M(T_N)/R = 0.9 \pm 0.2,$$

a relatively low value, consistent with the predominantly one-dimensional character of $Gd(OH)_3$. We shall discuss this in Sec. VII.

The most useful value of the thermodynamic functions is the energy at $T = 0$ K,

$$U_M(0)/R = -3.22 \pm 0.15 \text{ K},$$

since this provides a measure of the energy of the magnetically ordered ground state. We shall see (Sec. VII) that this value is consistent with our approximate ground state and it shows that the true ground state cannot be too different from our simple model.

D. Field Dependence of the Magnetic Specific Heat

In connection with the analysis of the high-frequency susceptibility to obtain the magnetic specific heat (Sec. IV A 2), it was shown that one could generally expect C_M to be field dependent. For the simplest analysis we may keep H small and calculate the asymptotic value $C_M(0, T)$, as we have done above, but a measurement of the field dependence provides additional and independent information on the interactions. In Fig. 4 we show the variation of $C_M(H, T)T^2/R$ as a function of H^2 in fields up to 15 kOe at a temperature of 5.527 K, and it can be seen that the change under these conditions is quite large (~30%). According to Eq. (18) we would expect the leading term in the field dependence to be proportional to H^2, and this is verified by the results in Fig. 4. The variation for $H \lesssim 5$ kOe is seen to approach a straight line and the asymptotic slope may be estimated to be $K_1 = -0.0050 \pm 0.0005$ (K/kOe)^2. We shall show later (Sec. VI D 3) that this value is in good agreement with the value calculated from the final set of interaction parameters.

No attempt was made in the present experiments to study the temperature dependence of K_1, but in principle this should provide an independent and relatively accurate means of determining the parameters $B_{2\parallel}$ and $B_{3\parallel}$ which occur in the leading terms for the $1/T$ expansion of K_1 (see Sec. VI D 3).

E. Isothermal Susceptibility Measurements

It is convenient to discuss the low-frequency susceptibility measurements in three parts: (i) the high-temperature results (14.7–20.0 K) for χ_T, from which the leading terms in Eq. (3) can be extracted; (ii) the helium-temperature results for both $\chi_T^{\parallel}$ and $\chi_T^{\perp}$, from which the leading terms in the magnetic anisotropy expansion can be obtained; and (iii) the powder susceptibility results near T_N, which can be related to the nature of the ordered state.

1. High-Temperature Results

The analysis of high-temperature susceptibility measurements is notoriously difficult since it is generally dominated by the leading Curie-law term which gives no information about the interactions. The usual procedure is to plot $1/\chi_T$ as a function of T to find θ by extrapolation, but this can lead to sizeable errors if higher-order terms are significant. To make full use of the relatively high accuracy of the present measurements we shall therefore plot $1/\chi_T T$ as a function of $1/T$ and we shall study the effect of the higher-order terms by an iterative procedure.

In Fig. 5 we show by the series of filled points the variation of $1/\chi_T^{\parallel} T$ as measured, corrected only for shape as explained in Sec. III B 1. It can be seen that the points fall on a fairly straight line and we might be tempted to associate the slope of this line with the leading term in Eq. (3), $-\theta_{\parallel}/\lambda$. However, this slope can be affected significantly by the inclusion of higher-order terms in the series expansion [Eq. (3)], and estimating $B_{2\parallel}$ and $B_{3\parallel}$ from the final set of interaction parameters (Sec. VI B) we can calculate

$$(1/\tilde{\chi}_T^{\parallel} T) = (1/\chi_T^{\parallel} T) - (B_{2\parallel}/T^2 + B_{3\parallel}/T^3)/\lambda, \qquad (25)$$

which should be a much better approximation to $(1 - \theta_{\parallel}^{\infty}/T)/\lambda$. Using $B_{2\parallel} = 2.05 \pm 0.10$ K^2 and $B_{3\parallel} = -0.59 \pm 0.10$ K^3 from Table II we then find the set of open circles in Fig. 5. It can be seen that the points again fit a straight line and we may assume that this is now close to the limiting high-temperature asymptote since the effect of additional higher-order terms (which can be roughly estimated from lower-temperature data, see Sec. VI D 2) is probably quite small. This is also confirmed by

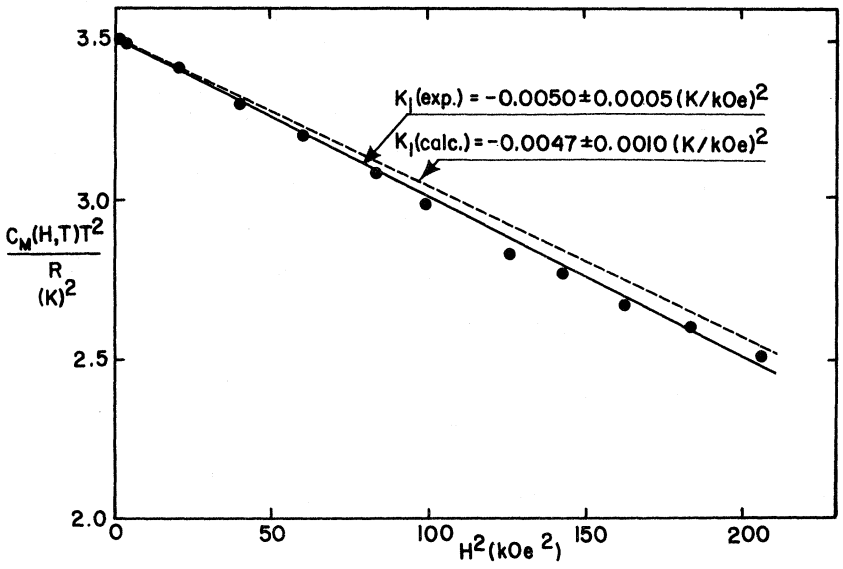

FIG. 4. Field dependence of $C_M(H,T)T^2/R$ for $Gd(OH)_3$ at $T = 5.527$ K as calculated from Eq. (18) from measurements of $\chi'(0)/\chi'(H)$. The dotted line has a slope $K_1 = -0.0047 \pm 0.0010$ (K/kOe)^2 as determined from theory [Eq. (30)], using the calculated expansion coefficients in the susceptibility given in Table II. The best fit to the low-field data gives $K_1 = -0.0050 \pm 0.0005$ (K/kOe)^2 as shown in the solid line, in excellent agreement with the calculated value. The small discrepancies between calculated and measured values at the highest fields are due to the limited expansions used for both the field and interaction terms, as explained in the text.

the intercept corresponding to $1/T = 0$, 7.82 ± 0.08 emu K/mole, which is in excellent agreement with the expected value 7.815 ± 0.008 emu K/mole. From the slope of the line we find $\theta_{\parallel}^{\infty} = 0.08 \pm 0.08$ K, where the error limit has been estimated to include the uncertainty due to the higher-order terms as well as the experimental scatter. This value may be compared with the result of a similar analysis of the zero-field high-frequency measurements which covered a larger temperature range (4–70 K), but with somewhat larger experimental scatter[6]: $\theta_{\parallel}^{\infty} = -0.04 \pm 0.08$ K. It may be seen that the two values are consistent within their respective error limits, and we can combine them to give a final weighted average

$$\theta_{\parallel}^{\infty} = 0.02 \pm 0.10 \text{ K},$$

where we have increased the over-all error limits to allow for the possibility of a hidden systematic error in either the low- or high-frequency measurements.

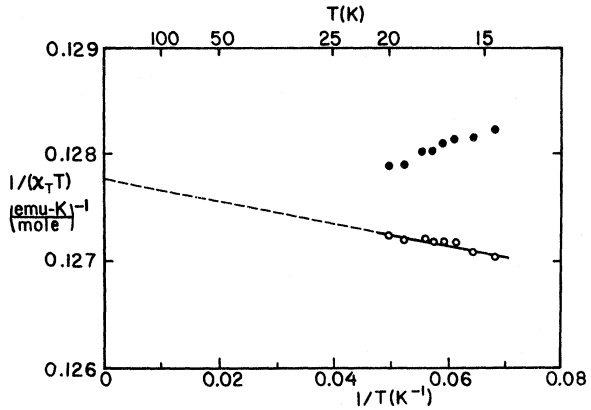

FIG. 5. Parallel susceptibility of $Gd(OH)_3$ measured in the liquid-hydrogen range and corrected to that of an infinite needle plotted as $1/\chi_T^{\parallel}T$ vs $1/T$ (solid circles) and as $(1/\tilde{\chi}_T^{\parallel}T) = (1/\chi_T^{\parallel}T) - (B_{2\parallel}/T^2 + B_{3\parallel}/T^3)/\lambda_v$ vs $1/T$ (open circles), with $B_{2\parallel}$ and $B_{3\parallel}$ taken from Table II. This "corrected" curve identifies the Curie–Weiss theta from the slope $\theta_{\parallel}^{\infty} = 0.08 \pm 0.08$ K, and the Curie constant from the intercept at $1/T = 0$: $\lambda = 7.82 \pm 0.08$ emu K/mole.

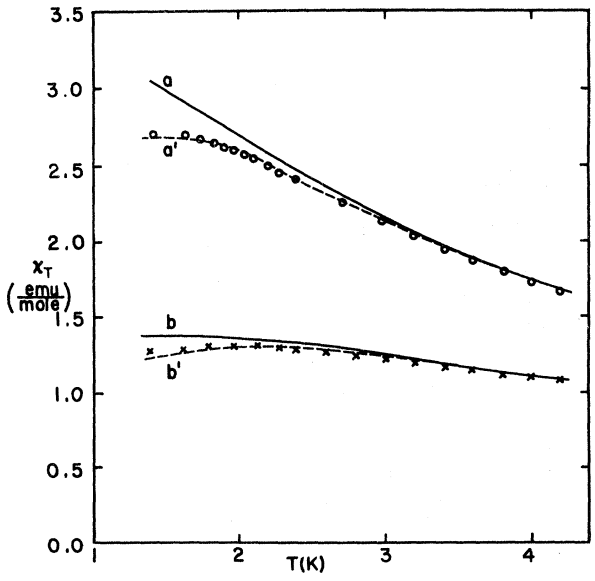

FIG. 6. Low-frequency susceptibility of $Gd(OH)_3$ for an infinitely long needle in the liquid-helium temperature range for measurements parallel (o) and perpendicular (×) to the c axis. Curves a and b are calculated from Eq. (3) with θ, B_2, and B_3 as found from Eqs. (6a)–(6c) and (7a)–(7c) (see Table II), using the final exchange constants in Table III. For the dashed lines one higher-order term B_4 has been included with $B_{4\parallel} = 1.1$ K^4 for curve a′, and $B_{4\perp} = 2.1$ K^4 for curve b′.

2. Anisotropy at Helium Temperatures

Measurements of the susceptibility parallel and perpendicular to the c axis were made on sample I (see Table I) from 1.4 to 4.2 K. The results corrected to correspond to an infinite needle according to Eq. (5b) are shown in Fig. 6. It can be seen that the susceptibility is quite anisotropic and this provides an additional variable which must be fitted by the final analysis.

The anisotropy can be expressed most conveniently in terms of the function $\Delta(1/\chi_T) = (1/\chi_T^{\perp}) - (1/\chi_T^{\parallel})$, and using Eq. (3) we would expect this to follow a law of the form

$$\Delta(1/\chi_T) = 1/\lambda(-\Delta\theta + \Delta B_2/T + \Delta B_3/T^2 + \cdots), \qquad (26)$$

where $\Delta\theta = \theta_{\perp}^{\infty} - \theta_{\parallel}^{\infty}$, $\Delta B_2 = B_{2\perp} - B_{2\parallel}$, and $\Delta B_3 = B_{3\perp} - B_{3\parallel}$. Experimental values of $\Delta(1/\chi_T)$ can be calculated from the data shown in Fig. 6, and plotting the results as a function of $1/T$ we obtain Fig. 7. At first sight, it looks as if this has the form predicted by Eq. (26) with only the two first coefficients $\Delta\theta$ and ΔB_2 contributing. However, fitting these to the data over the whole temperature region would in fact lead to sizeable errors, as we shall later see that higher-order terms are quite significant at the lower temperatures (Sec. VI D 1). To eliminate the effects of these higher-order terms, we therefore used an iterative procedure,

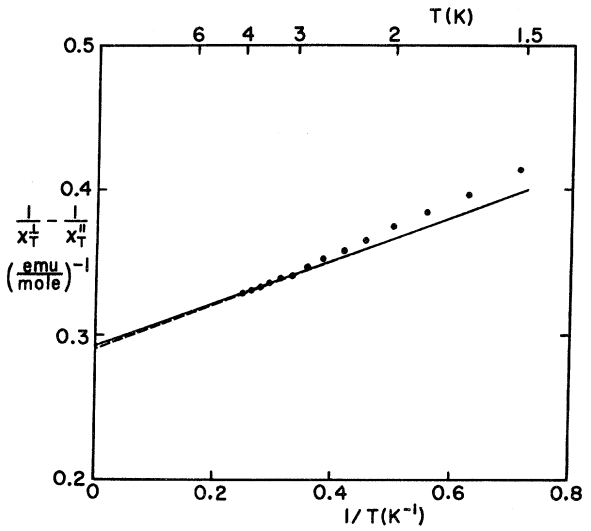

FIG. 7. Quantity $\Delta(1/\chi_T) = 1/\chi_T^{\perp} - 1/\chi_T^{\parallel}$ vs $1/T$ for $Gd(OH)_3$ corresponding to an infinitely long needle parallel to the c axis. The points have been determined graphically from the measurements shown in Fig. 6. The solid line is the least-squares asymptotic high-temperature fit to the data which gives $\Delta\theta = -2.29 \pm 0.10$ K and $\Delta B_2 = 1.15 \pm 0.15$ K^2. The dotted line is calculated from Eq. (26) using the values for the coefficients in Table II, as calculated from the exchange constants in Table III.

successively deleting low-temperature points, refitting $\Delta\theta$ and ΔB_2 to the remaining data, and extrapolating the results to $1/T = 0$. This procedure finally gives $\Delta\theta = -2.29 \pm 0.10$ K and $\Delta B_2 = 1.15 \pm 0.15$ K^2. We shall compare these values with the corresponding values calculated on the basis of the final analysis in Sec. VI D 2.

3. Powder Susceptibility near T_N

The results of the powder susceptibility measurements are shown in Fig. 8. The most prominent feature is the inflexion which occurs near 0.94 K, the temperature at which the specific heat has its sharp peak. Fisher has shown[68] on quite general grounds that such behavior is characteristic of the onset of antiferromagnetic long-range order, and he has proposed the explicit relation

$$\frac{C_M}{R} = A(T)\frac{\partial}{\partial T}(\chi_T T), \qquad (27)$$

where $A(T)$ is a slowly varying function of T.

In the original derivation, χ_T was defined as the susceptibility parallel to the direction of the spin alignment and only interactions between nearest neighbors on a simple two sublattice system were considered. Under these conditions $A(T)$ can be related to the total internal energy $U_M(0)$ and the asymptotic high-temperature susceptibility $(\chi_T T)_{T\to\infty}$:

$$A(T) = -f(T)U_M(0)/R(\chi_T T)_{T\to\infty}, \qquad (28)$$

where $f(T)$ is now a slowly varying function of T of order unity. In more complex systems with longer-range interactions, $f(T)$ will generally differ from one, and we can similarly include contributions from other components of χ_T.

Differentiating the results[69-71] in Fig. 8 and comparing $\partial(\chi_T T)/\partial T$ with the measured specific heat (Fig. 2), we find a function $A(T)$ which varies slowly with T, as expected, from a value of about 0.61 (emu/mole)$^{-1}$ at 0.7 K to about 0.72 (emu/mole)$^{-1}$ at 0.9 K. Substituting the previously determined values of $U_M(0)/R$ (Sec. V C) and $(\chi_T T)_{T\to\infty} \equiv \lambda$ (Sec. III B 1) we can thus find the corresponding $f(T)$, and in particular we find $f(T_N) = 1.8 \pm 0.2$. This value appears to be quite reasonable and there would seem to be no doubt that $Gd(OH)_3$ is an antiferromagnet with predominantly but not exclusively nearest-neighbor interactions.

F. High-Field Magnetization Measurements

Magnetization measurements were made parallel and perpendicular to the c axis, and the results for two temperatures (the highest and lowest measured) are shown in Figs. 9(a) and 9(b). As explained previously (Sec. III B 2), it is difficult to extract useful parameters from these measurements and the main purpose was therefore to provide a check

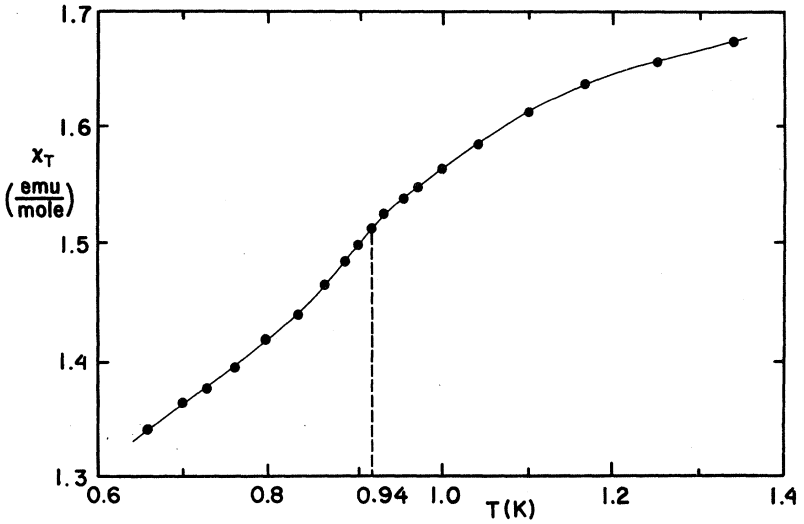

FIG. 8. Powder susceptibility of $Gd(OH)_3$ from 0.6 to 1.4 K. The curve clearly exhibits an inflection point near 0.94 K, the temperature of the specific-heat anomaly. These susceptibility data are later used to identify the anomaly as due to a paramagnetic to antiferromagnetic phase transition.

on some of the other results.

In particular, it was possible to compare the initial slopes with the results of the low-field susceptibility measurements, and in all cases good agreement was obtained. Another, more useful check provided by these results was for the approximate theoretical expression [Eq. (11)], which was used in the evaluation of the high-frequency specific-heat measurements. This expression with the final set of parameters taken from Table II is shown as the solid line in Figs. 9(a) and 9(b), and it can be seen that the agreement is very good for fields below about 7 kOe for $T = 4.212$ K. This is well within the range of fields used in the specific-heat measurements at these temperatures, and we can expect even better agreement at higher temperatures. The discrepancies at the highest fields are not at all surprising, since under these conditions many additional terms in the series expansion will become significant. Because of the large spin and relatively complicated interactions, it would be quite hard to calculate a much more exact high-field approximation and it would probably not be particularly useful in the present range of temperatures.

Unfortunately, no magnetization measurements could be made below the ordering temperature where interesting field-induced effects would be expected.

One purely empirical feature which may be noted in the present results, is the inflexion in both the low-temperature-magnetization isotherms. Such inflexions have been observed before[52] and they are simply a consequence of a competition of different interactions and the effect of the magnetic field. In the present case the effect is quite marked because a significant amount of short-range order develops [See Sec. VII B] before the final onset of long-range order.

VI. DETERMINATION OF THE INTERACTION CONSTANTS

A. Fitting Procedure

As explained in Sec. III A, we shall assume that there are three unknown interaction constants (J_1, J_2, and J_3) and we shall determine these by fitting the experimental results to the theoretical expressions given in Eqs. (6a), (15a), and (15b). However, this cannot be done in a straightforward way, since the analysis of the experiments themselves requires knowledge of some of the higher-order expansion coefficients, and these must first be estimated either empirically or theoretically. In both cases this involves an iterative procedure which must be applied with care if accuracy is desired in the final analysis. Such an iterative procedure is often omitted on the grounds that higher-order terms are probably small, but this is certainly not always the case.

The prime input data for our final fit will be $\theta_{\parallel}^{\infty}$, C_2, and C_3 and approximate values of these can be obtained by assuming that the higher-order terms $B_{2\parallel}$, $B_{3\parallel}$, C_4, C_5, etc., are in fact negligible. Solving Eqs. (6a), (15a), and (15b) one can then obtain an approximate set of values for J_1, J_2, and J_3, and using Eqs. (6b) and (6c) one can thus obtain estimates for $B_{2\parallel}$ and $B_{3\parallel}$. Using these, one can then obtain an improved estimate for $\theta_{\parallel}^{\infty}$, as discussed in Sec. V E, and substituting this together with the estimates of $B_{2\parallel}$ and $B_{3\parallel}$ into Eq. (18) one can thus obtain a more accurate determination of C_M. This then provides the starting point for the next step in the fitting procedure.

The next step involves estimating the effect of the previously neglected coefficients C_4, C_5, etc., which in contrast to $B_{2\parallel}$ and $B_{3\parallel}$ cannot be calculated from the preliminary J's, since the lattice sums involved in these particular coefficients are pro-

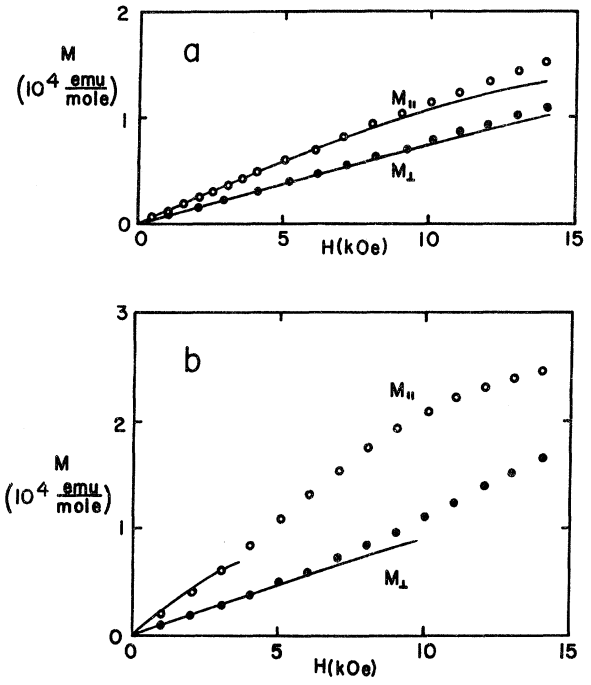

FIG. 9. Measurements of the parallel and perpendicular magnetization of $Gd(OH)_3$ vs external field for (a) $T = 4.212$ K and (b) for $T = 1.10$ K. The lines indicate the calculated magnetization using the approximate low-field expression in Eq. (11) with the expansion coefficients found from the final values of the exchange interactions (Table II). The agreement is good in (a) except for the highest fields, confirming the adequacy of the form for M and the final exchange constants. The discrepancies at the highest fields in (a) and (b) are due to failure to include more than one saturation term in M and also including the interactions only to first order in this term.

hibitively complex. To estimate the effect of these terms we have therefore adopted an empirical approach in which we have fitted the entire set of C_M data (calorimetric and high-frequency) to expressions of the form of Eq. (13), including successively two, three, four, and five terms. It was found that the addition of terms beyond C_4 had only a minor effect on the fitted values of C_2 and C_3, and it was therefore possible to determine these coefficients with some certainty. Omission of C_4, on the other hand, led to significant changes in C_2 and C_3 (about 2 and 20%, respectively), emphasizing the care which must be taken in determining the asymptotic terms.

The whole fitting procedure described above was repeated until a consistent set of expansion coefficients was obtained, and in practice this was achieved after about 20 iterations. The entire iterative procedure is illustrated schematically in Fig. 10 and it was carried out in practice using the Yale IBM 7040-7094 computer.

B. Results of Analysis

The final set of fitted values is shown in Table II which includes estimated error limits to allow for uncertainties in the experiments and the lattice sums, as well as the effect of truncating the susceptibility and specific-heat series.

It can be seen that the three principal coefficients $\theta_{\parallel}^{\infty}$, C_2, and C_3 are determined quite accurately, and we might therefore expect a correspondingly precise determination of the corresponding J's. This did in fact turn out to be the case, ultimately, but not before an interesting ambiguity was removed in the analysis.

This arose from the fact that J_2 and J_3 in $Gd(OH)_3$ happen to be much smaller than J_1, and with even a small uncertainty in the series-expansion coefficients, more than one solution for J_2 and J_3 is then possible. This might have been missed in a straightforward least-squares-minimization procedure, since each of the solutions had a well-defined local minimum, which would have appeared to be quite acceptable in the absence of other information.

However, closer study showed that there were in fact two (and probably no more than two) distinct minima; one corresponding to the solution $J_2 = -0.017 \pm 0.005$ K, $J_3 = 0.004 \pm 0.005$ K, and the other to the solution $J_2 = 0.010 \pm 0.005$ K, $J_3 = -0.020 \pm 0.005$ K, with J_1 essentially the same for both

TABLE II. Fitted susceptibility and specific-heat series-expansion coefficients.

Parameter	Value	Method of determination
$(\theta_{\parallel}^{\infty})^a$	0.02 ± 0.10 K	b
$B_{2\parallel}$	2.05 ± 0.10 K^2	c
$B_{3\parallel}$	-0.59 ± 0.10 K^3	d
$(\theta_{\perp}^{\infty})^a$	-2.26 ± 0.10 K	e
$B_{2\perp}$	3.22 ± 0.10 K^2	f
$B_{3\perp}$	-0.60 ± 0.10 K^3	g
C_2	4.09 ± 0.05 K^2	h
C_3	-4.2 ± 0.7 K^3	h
C_4	4 ± 2 K^4	i
C_5	-1 ± 3 K^5	j
C_6	-2 ± 6 K^6	k

[a] For an infinite needle parallel to the c axis.
[b] Average of two analysis of $1/\chi_T^{\parallel}T$, using iteratively estimated values of $B_{2\parallel}$ and $B_{3\parallel}$ (Sec. V E 1).
[c] Calculated from Eq. (6b) using iteratively fitted J's.
[d] Calculated from Eq. (6c).
[e] Calculated from Eq. (7a).
[f] Calculated from Eq. (7b).
[g] Calculated from Eq. (7c).
[h] Fitted to C_M measurements [Eq. (13)], using successively two, three, four, and five terms.
[i] Same as h using three, four, and five terms.
[j] Same as h using four and five terms.
[k] Same as h using all five terms.

and given by $J_1 = 0.180 \pm 0.005$ K. The rms deviation corresponding to the range of experimental uncertainties was about the same for both solutions and to distinguish between them it was therefore necessary to invoke additional physical information.

This was provided by the EPR experiments on pairs of Gd^{3+} ions in $Y(OH)_3$ and $Eu(OH)_3$.[18] These gave J_2 values of -0.0086 ± 0.0001 K and -0.0210 ± 0.0001 K, respectively, and interpolating of pure $Gd(OH)_3$ we can conclude that the first of the above two solutions must be correct. This also seems reasonable on physical grounds, since we would expect $|J_2|$ to be significantly larger than $|J_3|$ in view of the considerable difference in the respective lattice separations (see Fig. 1). A further piece of evidence favoring the first solution will become apparent in Sec. VID.

Our final solution for the J's is summarized in Table III, which also includes the corresponding values of the dipolar constants $\alpha_n = g^2\mu_B^2/r_n^3$. It can be seen that the uncertainty in J_3 includes the value $J_3 = 0$, as we had suspected at the outset, and it helps to confirm our supposition that the exchange coupling between more distant neighbors will indeed be very small. For the sake of consistency we shall use the small finite J_3 given by the least-squares fit for all further discussion, but there would be no significant difference if we chose to use instead the value zero.[72]

Much more important is the contribution of the magnetic dipole-dipole coupling which turns out to be only somewhat smaller than the exchange coupling for the near neighbors, and being proportional to $1/r^3$ remains quite appreciable for many of the more distant neighbors. We shall see the importance of these longer-range terms in Sec. VII, in which we shall consider the problem of the ordered state.

C. Graphical Analysis

If we assume that J_3 is in fact negligibly small, we can replace the final computer fit of J_1 and J_2 to $\theta_{\parallel}^{\infty}$, C_2, and C_3 by a graphical method which has the advantage of giving a ready insight into the importance of the different experimental uncertainties, and it also provides a convenient plot for comparing other experimental results with the final fit. This is shown in Fig. 11 in which we have plotted the expressions for $\theta_{\parallel}^{\infty}$, C_2, and C_3 given in Eqs. (6a), (15a), and (15b) as a function of J_1 and J_2, putting $J_3 = 0.004$ K and using the "experimental" values given in Table II. Corresponding to the experimental uncertainties, each term sweeps out a band of values and the final solution must lie within the area covered simultaneously by all the bands. It can be seen that the final computer fit, shown in the figure by P, satisfied this condition, as it must.

If J_3 had not been so small, we could have drawn a series of such figures for different values of J_3 until the proper simultaneous fit is obtained. The procedure of taking successive sections with one of the parameters held fixed can be very useful when, as in the present case, one of the parameters (here J_1) is well determined, but there is some uncertain-

TABLE III. Exchange and dipolar interaction constants for $Gd(OH)_3$.

Neighbor[a] n	Distance[a] r_n(Å)	Exchange constant[b] $J_n(K)$	Dipolar constant[b,c] $\alpha_n(K)$
1	3.61	0.180 ± 0.005	0.0525 ± 0.0004
2	4.06	-0.017 ± 0.005	0.0369 ± 0.0003
3	6.30	0.004 ± 0.005	0.00989 ± 0.00005
≥ 4	≥ 6.52	~ 0[d]	$(2.472 \pm 0.002)/r_n^3$[e]

[a]Relative to any arbitrary spin taken as origin (see Fig. 1).

[b]As defined in Eq. (1). The crystal field and higher-order interaction terms are estimated to be completely negligible except for b_2^0 which makes a small contribution ($b_2^0 = -0.02 \pm 0.01$ K).

[c]Calculated from $g^2\mu_B^2/r_n^3$ using lattice parameters given in Sec. IIA and $g = 1.992 \pm 0.001$ (Sec. IIIA).

[d]Assumed to be negligible.

[e]α_n in K when r_n is units of Å.

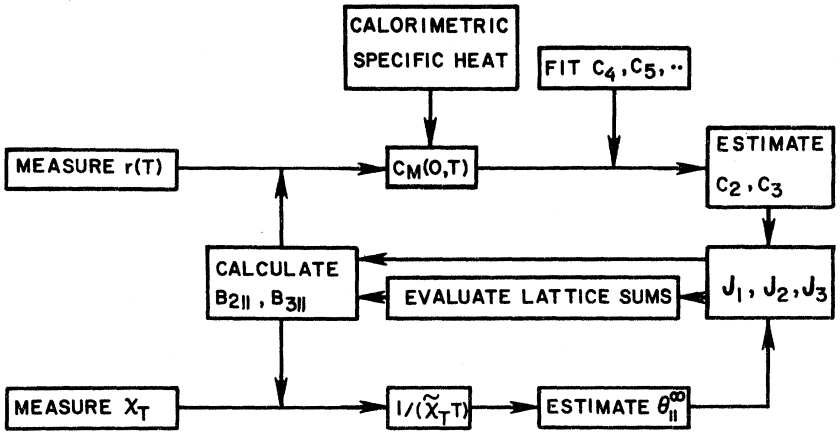

FIG. 10. Flow chart for determination of the interaction constants as explained in text.

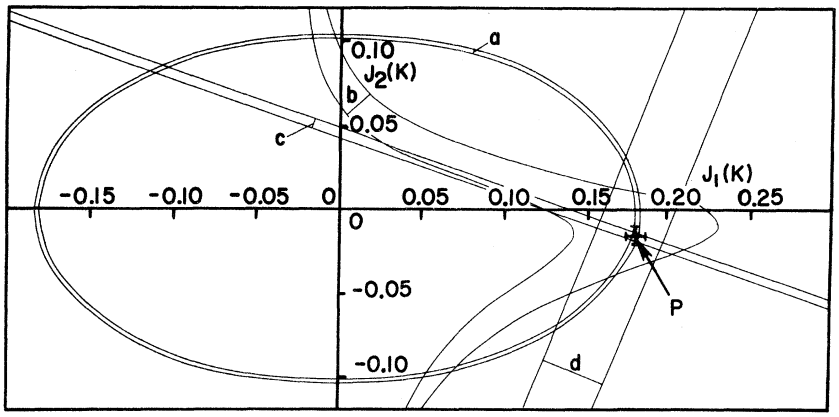

FIG. 11. Graphical solution for the exchange constants J_1 and J_2 from the high-temperature series-expansion coefficients assuming $J_3 = 0.004$ K. (The curves would not be visibly different if we would set $J_3 = 0$ or indeed anywhere within the range 0.004 ± 0.005 K.) The bands in the figure include all of the solution within the error limits of the expansion coefficients given in Table II as determined from Eq. (15a) for $C_2 = 4.09 \pm 0.05$ K^2 (band a); Eq. (15b) for $C_3 = -4.2 \pm 0.7$ K^3 (band b); Eq. (6a) for $\theta_{\parallel}^{\infty} = 0.02 \pm 0.10$ K (band c); and Eq. (29) for $B_{2\perp} - B_{2\parallel} = 1.15 \pm 0.15$ K^2 (band d). The region of simultaneous overlap corresponds to the computer solution given in Table III, as indicated by point P.

ty about the two remaining parameters. Thus a similar plot of J_2 vs J_3 for several fixed values J_1 close to the value indicated by the different computer solutions may be helpful in resolving questions about the possible number of solutions allowed within the experimental uncertainties.

Of course this method presupposes that we already have "experimental" values for the expansion coefficients $\theta_{\parallel}^{\infty}$, C_2, etc., and as we have seen this generally involves an iterative procedure which itself requires knowledge of the interaction parameters. However, it may often be possible to obtain reasonable estimates of the expansion coefficients from a purely empirical analysis of the data, and in such cases the present graphical method may then provide a simple and convenient way of solving for the individual interaction parameters.

D. Test of Fitted-Interaction Parameters

If the set of interaction parameters shown in Table III is indeed correct and complete, it should be useful for predicting observable properties which were not used in the fitting procedure. Such comparisons are useful for checking the over-all consistency of the analysis and they also provide confidence in the accuracy of some of the experimental methods.

1. Susceptibility at Helium Temperatures

Using the parameters in Table II we can calculate the variation of $\chi_T^{\parallel}$ and $\chi_T^{\perp}$ at temperatures well below those over which the fit to $\theta_{\parallel}^{\infty}$ was made, and in Fig. 6 we compare the results with the low-frequency measurements made at helium temperatures. In view of the fact that there are no adjustable constants in this comparison, the fit may be regarded as very satisfactory.

The small discrepancy at the lowest temperatures is readily explained by the omission of higher-order terms in the expansion and it can be removed by empirically adding one extra term for each direction: $B_{4\parallel} = 1.1 \pm 0.5$ K^4 and $B_{4\perp} = 2.1 \pm 1.0$ K^4. Such values are quite reasonable, though one should probably also consider other higher-order terms.

2. Anisotropy at Helium Temperatures

A more sensitive test is provided by the anisotropy of the susceptibility which may be characterized by the function $\Delta(1/\chi_T) = 1/\chi_T^{\perp} - 1/\chi_T^{\parallel}$. As shown in Sec. V E 2 this should follow a law of the form given in Eq. (26) with $\Delta\theta$ *independent* of the exchange interactions and determined only by the anisotropic terms in χ_T. Comparing the experimental value $(\Delta\theta)_{\text{expt}} = -2.29 \pm 0.10$ K (Sec. V E 2) with the value $(\Delta\theta)_{\text{calc}} = -2.28 \pm 0.14$ K calculated on the basis of magnetic dipole and crystal field interactions, we can see that any neglected anisotropic interactions must in fact be very small.

We can also compare the measured and calculated values of next-order term in the expansion of $\Delta(1/\chi_T)$, ΔB_2. On the basis of Eqs. (6b) and (7b) this should be given by

$$\Delta B_2 = 7.04 J_1 - 3.02 J_2 - 1.99 J_3 - 0.13, \qquad (29)$$

and equating this to the experimental value $(\Delta B_2)_{\text{expt}} = 1.15 \pm 0.15$ K^2 (Sec. V E 2), we can plot another "band" in the exchange-parameter plot. If we assume that $J_3 \simeq 0.004$ K, we obtain the two lines shown in Fig. 11, and it can be seen that they are indeed consistent with the previously obtained results. A similar comparison assuming the second solution with $J_2 \simeq 0.010$ K and $J_3 \simeq -0.020$ K shows no such consistency, and this provides additional evidence for the first solution.

3. Field Dependence of C_M

As discussed in Sec. VD, no systematic study was undertaken of the field dependence of C_M, but we do have quite an accurate value for K_1, the coefficient of the leading term in H^2 at one temperature $T' = 5.527$ K. This may be compared with the value calculated from the expression given by the series expansion [Eqs. (6a)–(6c)]

$$K_1(T) = \frac{-(\lambda/R)(B_{2\parallel} + 3B_{3\parallel}/T + \cdots)}{(T - \theta_\parallel + B_{2\parallel}/T + B_{3\parallel}/T^2 + \cdots)^2}, \qquad (30)$$

and substituting from Table II we obtain $[K_1(T')]_{\text{calc}} = -0.0047 \pm 0.0006$ $(K/\text{kOe})^2$, in excellent agreement with the experimental value $[K_1(T')]_{\text{expt}} = -0.0050 \pm 0.0005$ $(\text{K/kOe})^2$.

In more complex systems, a detailed study of the field dependence of C_M, and Eq. (18) in particular, could well be used to provide an important independent piece of information for determining the interaction parameters. In the present case it provides a convenient and gratifyingly accurate confirmation of the analysis previously used.

4. Comparison with EPR Pair Measurements

A series of very detailed EPR experiments has recently been reported[17–20] for Gd^{3+} pairs in $Y(OH)_3$ and $Eu(OH)_3$. These experiments show that the dominant anisotropic terms are indeed as given in Eq. (1) and in particular they show that anisotropic bilinear exchange must be very small. At the same time, they do indicate that there are some small additional *biquadratic* interactions of the form $Q^{|m|}(1,2)O_m^{(2)}(1)O_{-m}^{(2)}(2)$, with Q's of the order of 0.001 K, where the $O_m^{(2)}(i)$ are normalized spherical-tensor operators as defined by Smith and Thornley and others.[73–75] However, an extension of the expansion formulas to include terms of this kind shows that the contribution to both χ_T and C_M will be entirely negligible and it justifies our neglect of such terms in $\mathcal{H}'$.

The EPR experiments also give a measure of the isotropic interactions, and in earlier analyses these were simply interpreted in terms of the usual bilinear exchange constants J. However, the observation of anisotropic biquadratic interactions in the present case suggests that a biquadratic isotropic coupling of the form[76,77] $Q\sum(-1)^m O_m^{(2)}(1)O_{-m}^{(2)}(2)$ may perhaps also be present, and this is difficult to detect in the EPR experiments.[18] In fact, a detailed study of nearest-neighbor interactions has shown that the EPR experiments are most sensitive to a *linear combination* of J_1 and Q_1, and in the present case this combination happens to be $J_1' \approx J_1 - 41Q_1$. Values of J_1' were determined for nearest-neighbor pairs in both $Y(OH)_3$ and $Eu(OH)_3$, and interpolating to the $Gd(OH)_3$ lattice spacings we can estimate[78]

$$J_1' = 0.202 \pm 0.010 \text{ K}.$$

Similar analyses of the next-nearest-neighbor interactions in $Y(OH)_3$ and $Eu(OH)_3$ did not indicate any higher-order interactions[18] ($|Q_2| < 10^{-5}$ K), and again interpolating to the $Gd(OH)_3$ lattice spacings we can estimate[78]

$$J_2 = -0.017 \pm 0.004 \text{ K}.$$

These values may be compared with the J's given in Table III and we may note a very satisfactory similarity. In particular we can now verify that the isotropic biquadratic term in J_1' must in fact be quite small and we can estimate

$$Q_1 = -(5 \pm 6) \times 10^{-4} \text{ K}.$$

We may thus conclude that the biquadratic coupling in $Gd(OH)_3$ is indeed very small, as we might have guessed. However, in the absence of any quantitatively reliable theory for the interactions such a conclusion cannot be regarded as trivial, and it provides an important piece of information on the adequacy of the Hamiltonian given in Eq. (1).

E. Characteristics of the Results

The results for $Gd(OH)_3$ are in many respects very similar to those found in other systems of interacting S-state ions. Two factors make $Gd(OH)_3$ relatively simple to analyze: the dominance of the isotropic nearest-neighbor exchange, and the unusually small crystal field. On the other hand, the magnetic dipole interactions are relatively more important, and in Sec. VII we shall see how they may actually dominate the nature of the ordered state. $Gd(OH)_3$ is thus both simpler and more complex than other similar systems and it certainly warrants a detailed study of its cooperative properties. The results obtained up to this point have established the *form* and *magnitude* of all the significant interactions with some accuracy and we have therefore reached the point at which the more interesting, and in this case, much more difficult, cooperative problem can be formulated unambiguously. In Sec. VII we shall consider this problem briefly, but we shall quickly see that the solution is by no means trivial, and even though the complete Hamiltonian is known with unusual certainty a considerable amount of additional work is still required.

VII. PROBLEM OF SPIN ORDERING IN $Gd(OH)_3$

A. Approximations to the Ground State

Given a completely determined spin Hamiltonian it is sometimes possible to write down an exact ordered ground state,[79] or at least an approximate ground state subject only to a small uncertainty due to zero-point motion.[80–82] The simplest cases are those in which one particular interaction is domi-

nant and responsible for producing an ordered state which can be visualized in terms of a self-consistent molecular-field picture.

Problems arise when the physically largest interaction is not sufficient by itself to produce long-range order. In such cases, competition between several of the weaker interactions may then result in relatively complex situations, and these are generally not easy to predict from knowledge of the Hamiltonian alone. Well-known examples of this type are the predominantly one- and two-dimensional antiferromagnets[83–86] and the isotropic fcc antiferromagnets.[87–93] It would appear that $Gd(OH)_3$ is another complex system of this kind.

From Table III we can see that by far the largest interactions in this system are those between nearest neighbors, but since these couple only spins within one-dimensional linear chains, they cannot by themselves produce long-range order. Of the interactions between the more distant neighbors several are comparable in magnitude, and we must therefore expect a subtle competition to determine the actual state of long-range order. As we shall see, this is further complicated by the high symmetry of the hydroxide lattice.

To find an approximate ground state we shall neglect the complication of zero-point fluctuation effects and we shall use simple molecular-field theory to estimate the energies of a few reasonable types of spin arrangements. We would hope that this might produce a good starting point for more accurate energy calculations, which will ultimately have to refine both the details of the actual sublattice structure and also improve on the approximations inherent in the molecular-field treatment.

1. Collinear Structures

From the sign of J_1 and the nature of the magnetic dipole interaction, we can immediately guess that the ground state can be reasonably approximated by some arrangement or modification of chains of antiparallel spins perpendicular to the c axis, as shown in Fig. 12. This arrangement minimizes the large interactions between nearest neighbors, and summing over all the spins in one chain it corresponds to a stable mean-field energy,[94] $E_{aa}(\phi_a) = -2.79 \pm 0.06$ K, independent of the angle ϕ_a specifying the orientation of the spins in the basal plane. In this approximation there is no first-order coupling between neighboring chains, since all the interactions average out to zero by symmetry, as may be seen in Fig. 13, and to obtain long-range order we have to consider the contribution of next-nearest-neighbor chains.

These are coupled only through relatively weak interactions, and since these are primarily due to magnetic dipole coupling they will be quite anisotropic. To obtain an estimate of this coupling, the

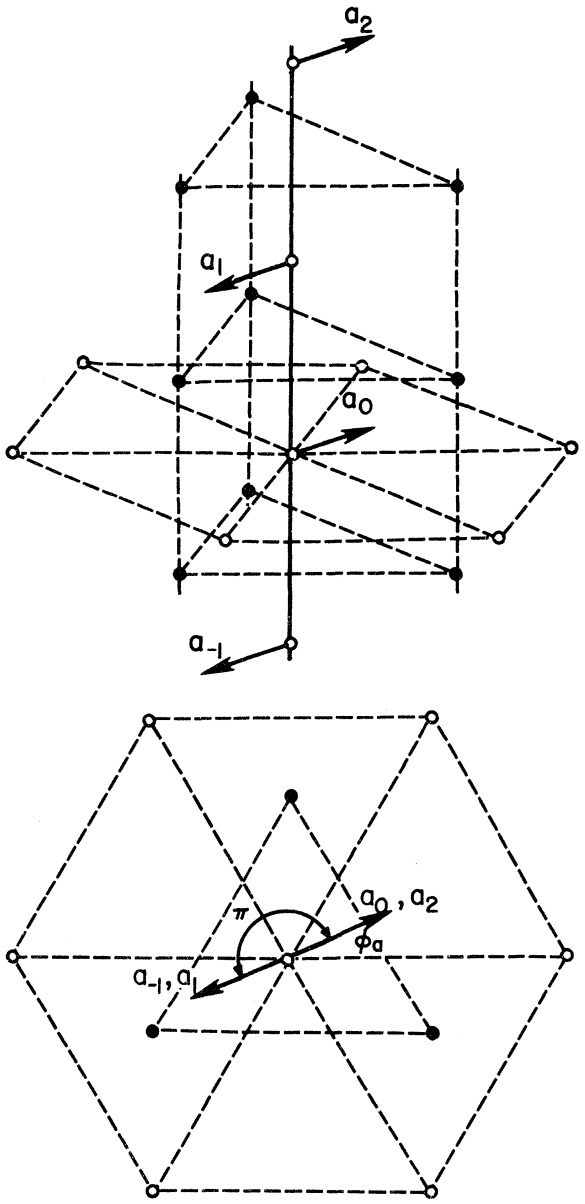

FIG. 12. Simple chain picture of $Gd(OH)_3$ as a first guess to the ordered state. The dominant nearest-neighbor antiferromagnetic exchange interaction combined with the dipolar interaction minimizes the energy with spins a_n antiparallel and perpendicular to the c axis. The total interaction energy between one spin and all remaining spins in the chain is independent on the phase angle ϕ_a.

energy of one particular configuration of two next-nearest-neighbor chains was calculated by evaluating the corresponding lattice sums. The configuration chosen corresponded to $\phi_a = \phi_c = \phi$, as shown in Fig. 14. The result was found to be $E_{aa} + E_{ac}(\phi, \phi)$ with $E_{ac}(\phi, \phi) = [0.03 \pm 0.02 - (0.04 \pm 0.02)\cos^2\phi]$ K, where the angle ϕ is measured relative to the interchain direction. We may note that $E_{ac}(\phi, \phi)$ is

very much smaller than the intrachain energy E_{aa}, but as we shall see, it may still be quite significant for the establishment of three-dimensional long-range order.[95,96]

Using this result we can now calculate the total energies of various types of simple spin arrangements consistent with the symmetry of the whole lattice. Two of these are illustrated in Figs. 15 and 16.

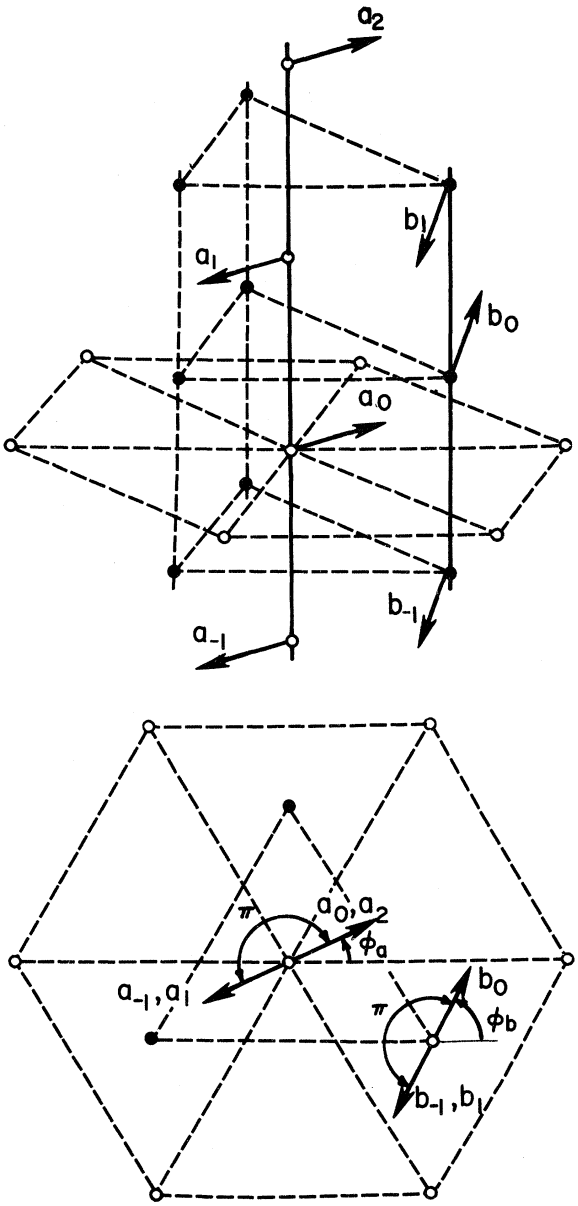

FIG. 13. Two *nearest-neighbor* chains aligned antiferromagnetically, as in Fig. 12. To first order there is no net interaction between two such chains for any orientation of the phase angles ϕ_a and ϕ_b, since interactions cancel identically by symmetry. (Consider, for example, the interaction of a_0 with pairs of symmetrically placed spins such as b_0 and b_{-1}.)

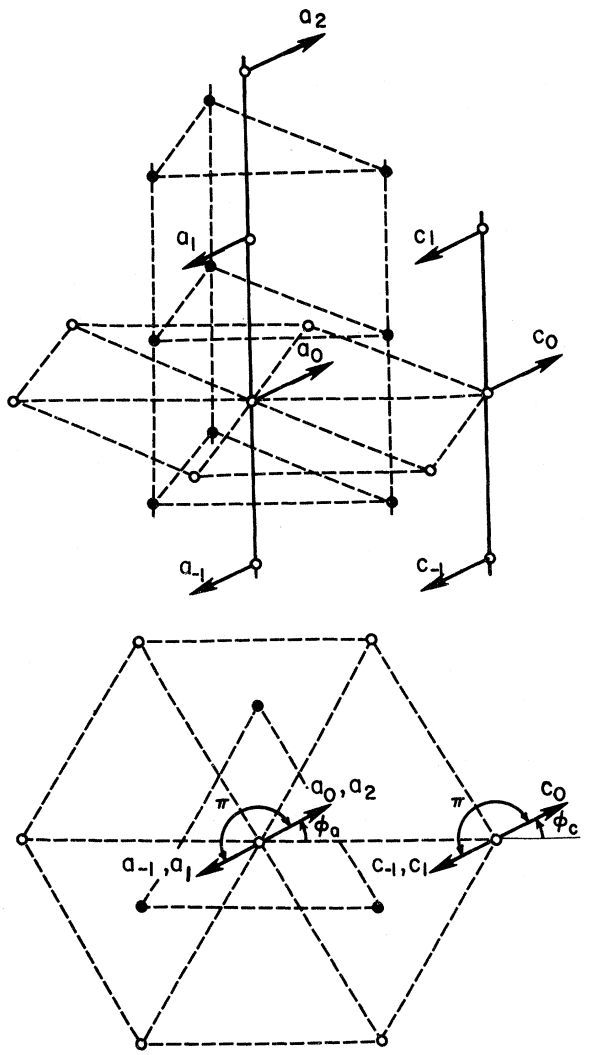

FIG. 14. Two *next-nearest-neighbor* chains aligned antiferromagnetically as in Fig. 12. The energy of interaction of two such chains depends on the phase angles ϕ_a and ϕ_c, $E_{ac}(\phi_a, \phi_c)$, and it will generally be quite anisotropic. To obtain an estimate of the typical next-nearest-neighbor chain interaction energies we consider the simple case $\phi_a = \phi_c = \phi$ shown here. For this we find $E_{ac}(\phi, \phi) = [(0.03 \pm 0.02) - (0.04 \pm 0.02) \cos^2\phi]$ K, as given in the text.

In the first one, which we shall denote as state I, we consider all spins in a given basal plane parallel and making an angle ϕ with one of the a axes. By symmetry the energy of this state must in fact be independent of ϕ, and summing over all chains we can estimate $E_I = -2.70 \pm 0.19$ K. This is *higher* than E_{aa}, the value for a single chain, and we are led to conclude that this particular configuration will probably not stabilize long-range order.[97] State II may be characterized by two pa-

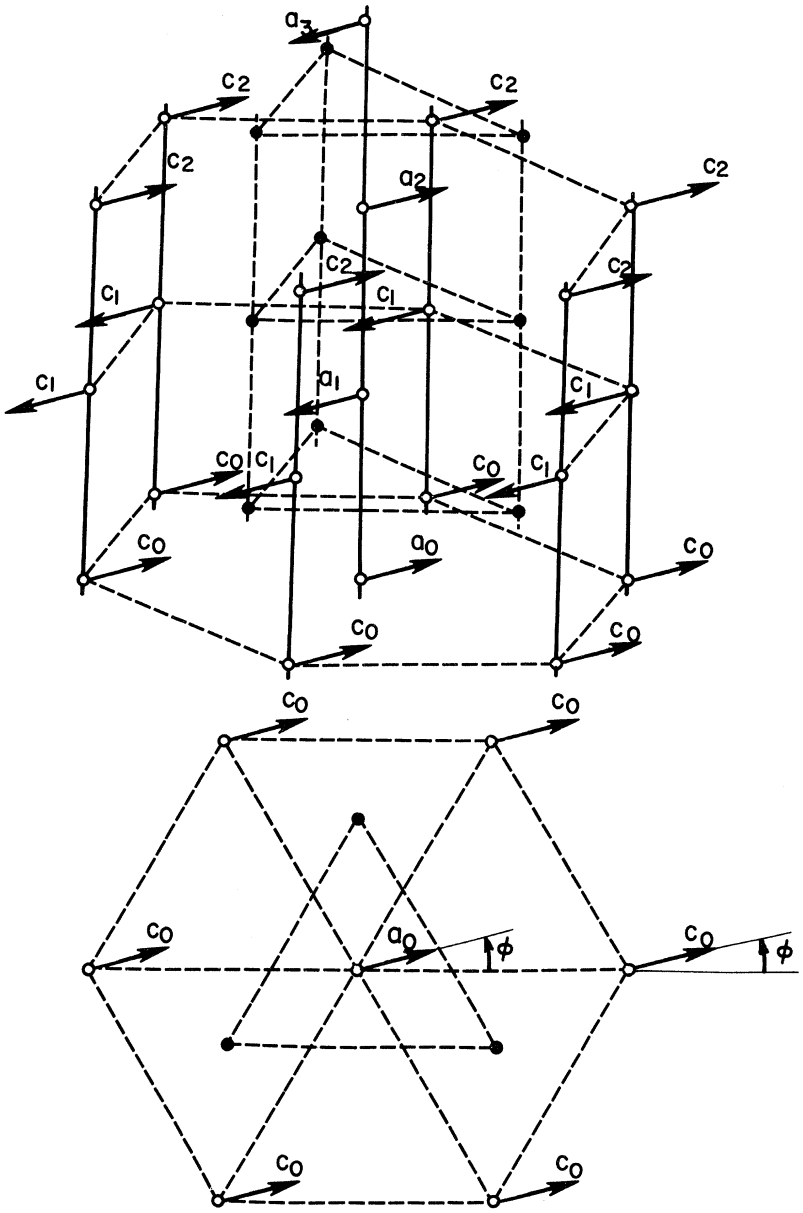

FIG. 15. Arrangement of spins in ordered state I, showing the spins (open circles with arrows) having a net interaction with one another. The remaining spins (shown as solid circles without arrows) form a second identical pair of antiferromagnetic sublattices which are uncoupled from the first pair to first order. In both pairs of sublattices, all spins in a given basal plane are parallel, and the energy is independent of the phase angle ϕ. With the interactions appropriate to $Gd(OH)_3$ this state is found to be unstable relative to the single-chain energy.

rallel and four antiparallel next-nearest-neighbor chains, and this has an angular dependence proportional to $\cos 2\phi$. The lowest energy corresponds to $\phi = 0$, as shown in Fig. 16, and has the value $E_{II}(0) = -2.89 \pm 0.09$ K. This is only slightly lower than E_I, but it is lower than E_{aa} and state II is therefore stable.

It is of course quite possible that some more complex arrangement of antiferromagnetically aligned linear chains might produce a somewhat lower energy, but it seems unlikely that this would result in any very significant reduction in the total energy, and in trying to improve our approach to the true ground state we shall therefore look for other kinds of modifications of the basic pattern which we have established so far.

2. *Simple Spiral States*

Staying for the present within the mean-field approximation, we note that the only way of lowering the total energy through the previously ineffective next-nearest-neighbor interaction, is to remove the strict cancellation imposed by the completely symmetrical arrangement of alternately antiparallel spins. There are many ways of relaxing this constraint, but perhaps the simplest is to allow the angle between successive spins along a chain to be somewhat different from π (say $\pi - \theta$), still keeping the spins in a plane perpendicular to the c axis. Such a flat helix will now have a finite inter-

action with a similar helix at the position of the *nearest-neighbor* chains, the energy depending on the spiral angle θ the relative phase angle between the two spirals (ϕ_{ab}) (see Fig. 17), and the strength of the interactions J_2, α_2, etc. If we make the reasonable first approximation that the second-nearest neighbors are dominant in determining the relative phase angle, we find $\phi_{ab} = \frac{1}{2}\pi$, and this is confirmed by minimizing the energy of all the interactions in two adjacent chains.

If we now assume the same relative phase angle between all nearest-neighbor chains, we obtain state III shown in Fig. 18, and carrying out the corresponding lattice sums[98] for different values of the angle θ, we can estimate the minimum energy $E_{III}(\theta = 13°) = -2.79 \pm 0.19$ K. It would appear that

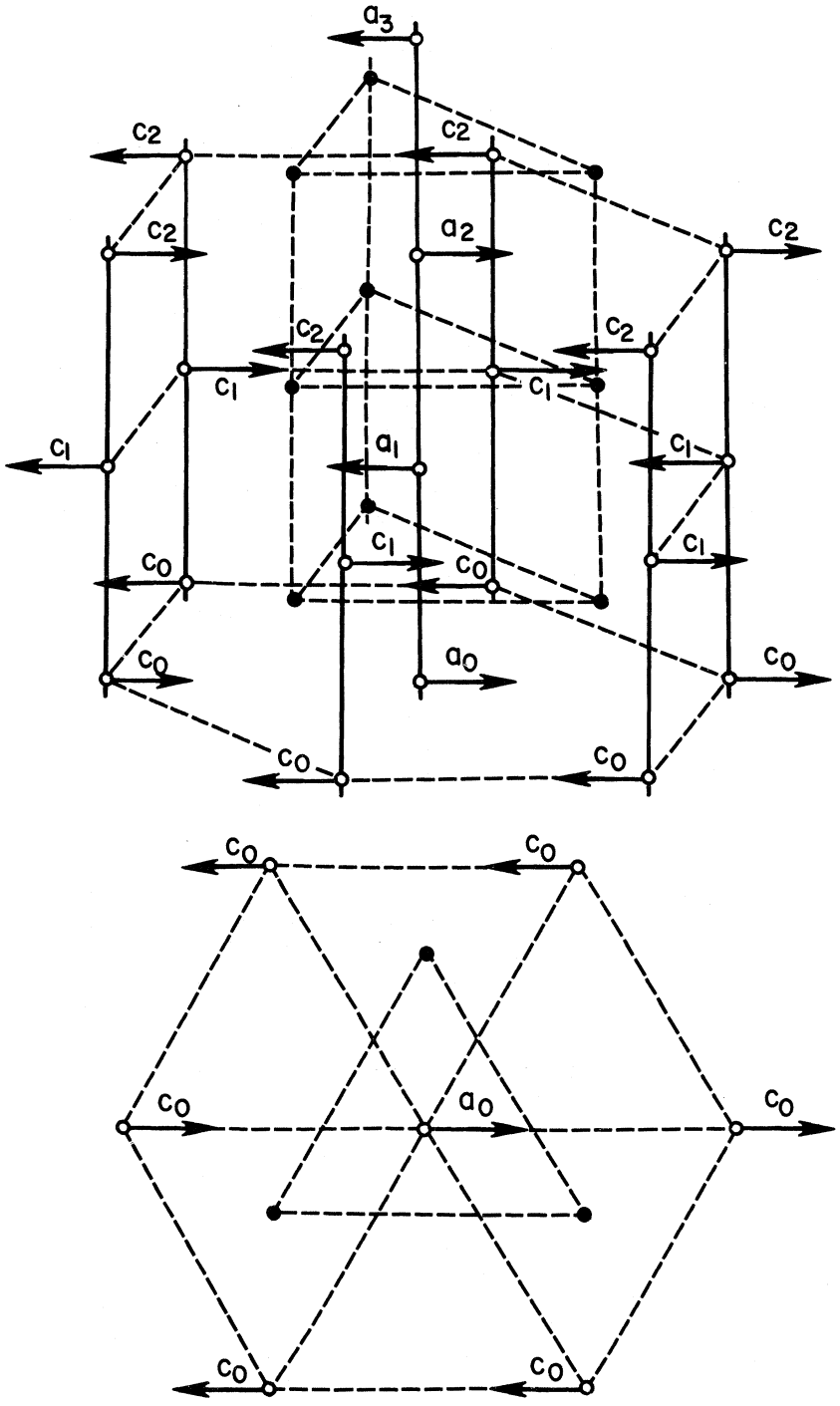

FIG. 16. Arrangement of spins in ordered state II. This is a modification of the state shown in Fig. 15, obtained by reversing the spins in four of the next-nearest-neighbor chains, consistent with the symmetry of the whole crystal. The energy of this state depends on the phase angle ϕ (see Fig. 12) and it has its minimum value for the case $\phi = 0$ shown here: $E_{II}(\phi = 0) = -2.89 \pm 0.09$ K. This is stable relative to the single-chain energy.

this energy is somewhat lower than that of state I, and not as low as that of state III, but the error limits overlap and it is really not possible to decide unambiguously which is closest to the actual ground state. The fact that all three states are so close to the mean-field energy of the isolated antiferromagnetic chains suggests that we are probably quite close *in energy* to the true ground state but not necessarily to the actual spin configuration, which could well be some even more complex modification of the basic patterns which we have considered here.

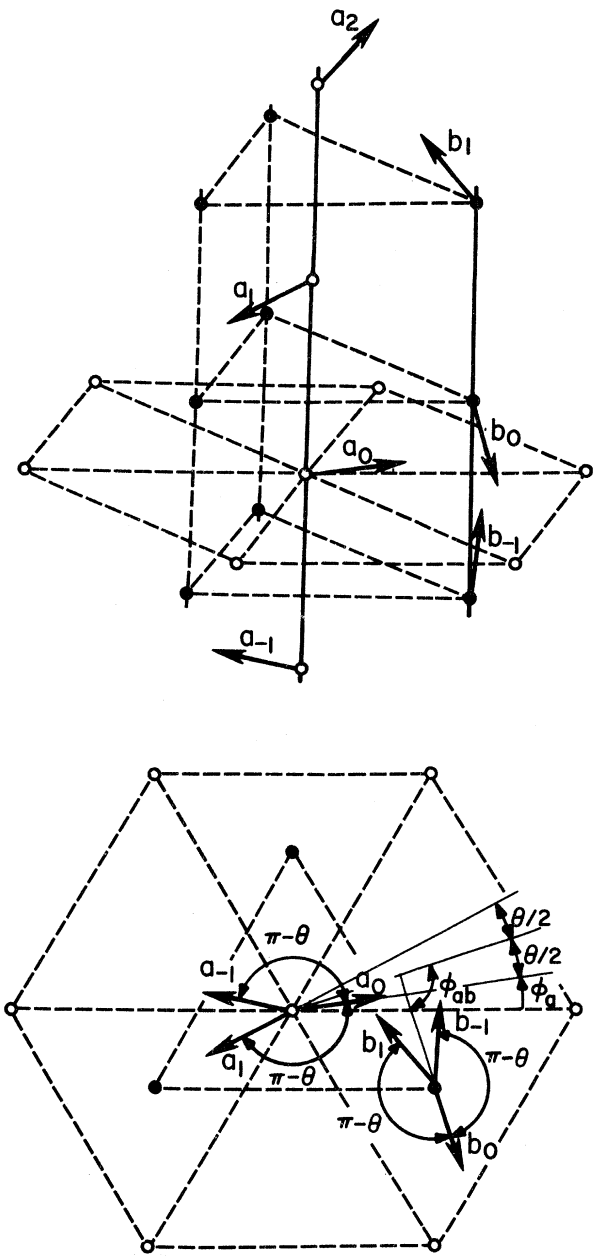

FIG. 17. Simple spiral state for nearest-neighbor chains. The spins in a plane are perpendicular to the c axis and the angle between successive spins along a chain is $\pi-\theta$. The interaction energy between the chains is a function of the spiral angle θ and the phase angle ϕ_{ab} between the chains as discussed in the text. The minimum energy is obtained with $\phi_{ab}=\frac{1}{2}\pi$.

Evidence that the energy estimate is approximately correct is provided by the experimental value of $U_M(0)/R = -3.22 \pm 0.15$ K (Sec. VC), which is almost within the calculated range of values for $E_{II} = -2.89 \pm 0.09$ K. This does not rule out more complex modifications of the ordered state which might lower the energy further, but we can be fairly certain that the energy associated with any such changes will be small compared with the terms which we have already found.

Possible modifications of the structure include spirals with spins no longer perpendicular to the c axis (e.g., restricted to a lie on a cone), or structures with more than one periodicity. Such complications have previously been observed in rare-earth metals,[99] but in those cases detailed analyses were hampered by lack of precise knowledge of the complete interaction Hamiltonians. We would hope that the rather complete information which we have been able to obtain on the interactions in $Gd(OH)_3$ would make this an unusually attractive case for further detailed study, even though it is clearly complex, involving competing effects of weak long-range interactions.

3. *Correlation Effects*

One complication which will have to be considered in any more detailed study is the possibility that correlation effects, which have been neglected in the present mean-field calculations, may make contributions to the energy which are comparable to the small energy gains resulting from more complex spin configurations. Since both the exchange and dipolar interactions have off-diagonal terms which are quite large, we must certainly expect a significant zero-point contribution to the ground-state energy, and this contribution will not cancel out even in the highly symmetric states. Unfortunately, it is not trivial to calculate the size of these effects, but this may be quite comparable to the weak long-range dipolar contributions and in a more detailed analysis they should certainly be considered.

4. *Further Experiments (?)*

For the present we can conclude that $Gd(OH)_3$ is almost certainly an antiferromagnet with spins approximately perpendicular to the c axis, even though there is little direct experimental evidence for this. Further study is clearly called for, and a number of possible experiments suggest themselves. These include neutron diffraction, NMR

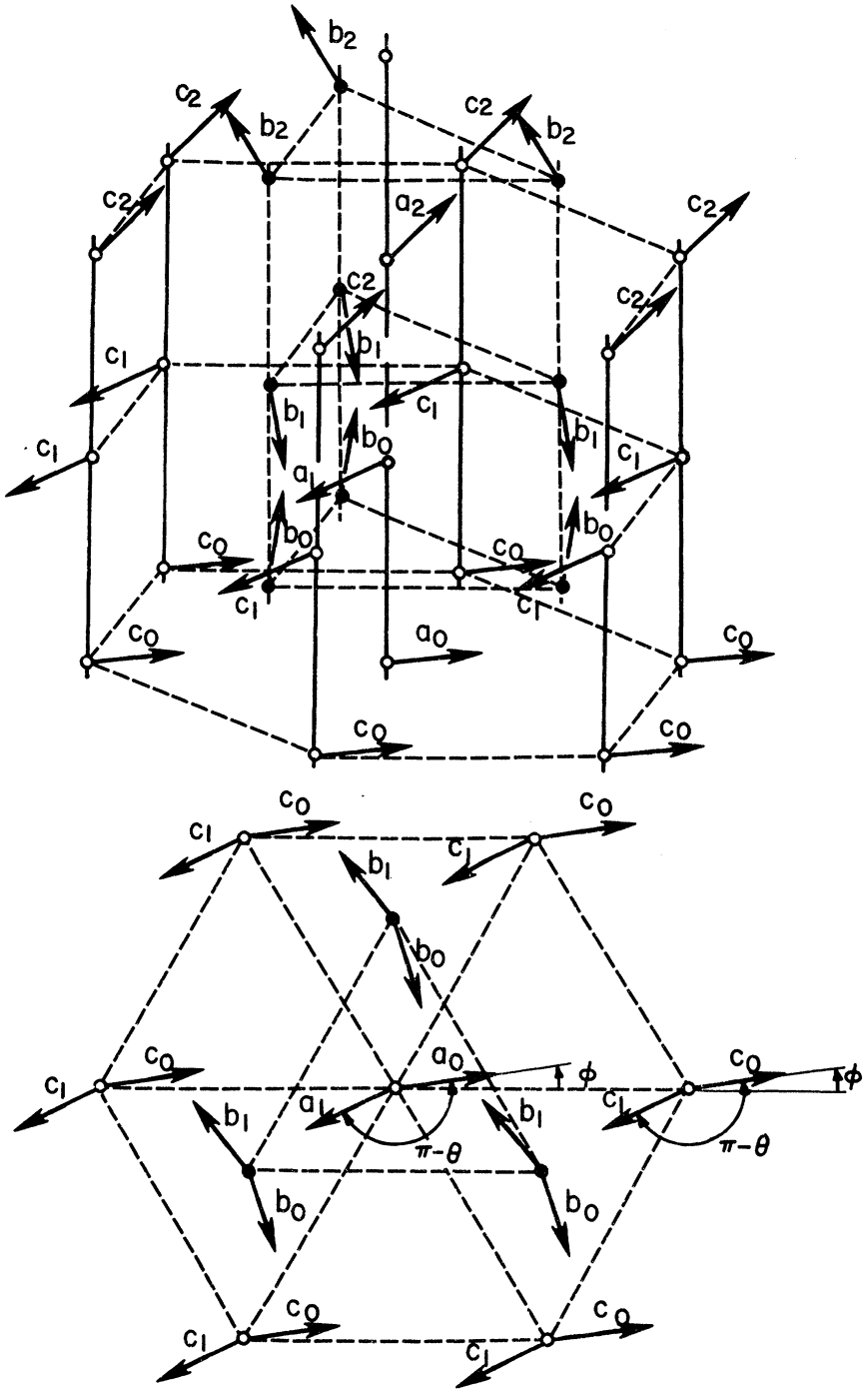

FIG. 18. Simple spiral state in Fig. 17 (with $\phi_{ab}=\frac{1}{2}\pi$) extended to all nearest-neighbor chains (state III). The total interaction energy is a function of θ and the minimum energy is obtained for $\theta=13°$; $E_{III}(\theta=13°) = -2.79 \pm 0.19$ K. This energy is not as low as that of state II (Fig. 16), but the uncertainty limits overlap and either could be a stable ground state. In reality the true ground state is probably more complex than either II or III, but its energy will probably not be very different.

on the protons of the OH^- groups, and a detailed single-crystal study of M and C_M as a function of H and T in the ordered state. However, the relatively low-ordering temperature, high neutron-absorption cross section of natural Gd, and the small size of the available crystals will make any of these quite difficult. Moreover, if the ordered state is really as complex as it would appear, a fairly detailed analysis will be required.

Perhaps a more promising first step would be an improvement of the present theory, using the fact that the complete Hamiltonian has been determined with unusual certainty. In any case, the problem of the ordered ground state of $Gd(OH)_3$ stands as a clearly defined challenge to both theory and experiment which may perhaps lead to further insight in-

to more general questions relating to competing interactions.

B. Region of the Phase Transition

In the absence of a clear picture of the ordered ground state, it is obviously impossible to give a detailed discussion of the onset of order, but we may note a number of qualitative features which can be understood in the light of the previous analysis.

Thus, the correspondence between C_M and $\partial(\chi_T T)/\partial T$ is now seen to be consistent with the behavior of a predominantly but not completely nearest-neighbor antiferromagnet. Similarly, the large amount of short-range order above T_N, as evidenced by the broad bump in the specific heat and the corresponding contribution to the entropy, is explained by the relative importance of the intrachain interactions, and the surprisingly low-ordering temperature is seen to be a result of the relatively weak *inter*chain coupling.

It is of interest to compare the observed ordering temperature $T_N = 0.94$ K with the value calculated on the basis of the molecular-field approximation for the "best" of the spin configurations (state II), considered above. In mean-field theory the relation between the energy per spin and T_N is given by[100]

$$(T_N)_{\mathrm{mf}} = -(E)_{\mathrm{mf}}[2(S+1)/3S], \tag{31}$$

and substituting for S and E_{II} we find

$$(T_N)_{\mathrm{mf,II}} = 2.47 \text{ K}.$$

It is not surprising that this is considerably higher than the observed T_N and in fact the discrepancy provides additional confirmation of the pseudo-one-dimensional character of $Gd(OH)_3$.

We are now also in a position to understand the striking difference between $GdCl_3$ and $Gd(OH)_3$. This can be seen to result from *two* changes in the corresponding exchange interactions: an increase in strength of the nearest-neighbor coupling and a *decrease* in the next-nearest-neighbor coupling. Such opposing changes appear puzzling at first, since $GdCl_3$ and $Gd(OH)_3$ are isostructural with both the c and a lattice constants about 14% smaller in the hydroxide. However, a recent analysis of a number of different Gd^{3+}-Gd^{3+} exchange constants has shown[19] that the interactions may themselves result from several competing contributions, so that the J's need not scale uniformly with homogeneous changes in the lattice distances. In $GdCl_3$ the ferromagnetic next-nearest-neighbor exchange just happens to dominate, while in $Gd(OH)_3$ the nearest-neighbor interactions have to combine with several weaker interactions to produce a complex antiferromagnetic state.

VIII. SUMMARY AND CONCLUSIONS

The principal results of the present study are the thermodynamic series expansion coefficients given in Table II and the corresponding microscopic interaction parameters given in Table III. From the consistency of several empirical cross checks we have been able to conclude that all other interactions must be quite small, and we have thus been able to determine the complete interaction Hamiltonian with unusual precision.

The largest single interaction is the nearest-neighbor isotropic exchange $J_1 = 0.180 \pm 0.005$ K, which tends to align nearest neighbors antiferromagnetically. The next-nearest-neighbor exchange is ferromagnetic but much smaller, $J_2 = -0.017 \pm 0.005$ K and the third-nearest-neighbor exchange is zero within the limits of error ($J_3 = 0.004 \pm 0.005$ K), consistent with the much larger separation in the lattice.

There is no theory at present to account for the magnitudes of the observed J's, but the three fitted parameters explain, within experimental error, an extensive series of magnetic and thermal measurements and they are consistent with independent EPR experiments on Gd^{3+}-Gd^{3+} pairs in diamagnetic host lattices.[17–20]

In addition to the isotropic exchange interaction, there is the usual magnetic dipole interaction, which can be calculated from the g factor and the lattice parameters. This turns out to be quite weak compared to the nearest-neighbor exchange interaction, but two factors make it unusually important in determining the properties of $Gd(OH)_3$. Firstly, it provides almost the entire source of anisotropy, the crystal field and anisotropic-exchange contributions being negligible in comparison. Secondly, it provides a means of coupling the more distant neighbors and this may turn out to be decisive in choosing between different possible ordered states.

The problem of long-range order is complicated by the predominantly linear-chain character of the interactions (nearest-neighbor exchange plus dipole), which would favor an antiferromagnetic arrangement with spins perpendicular to the c axis. Such a one-dimensional system is of course not stable, but to couple neighboring chains one either has to remove the first-order cancellation imposed by the high symmetry of the hydroxide lattice or invoke longer-range interactions.

Both these possibilities have been considered briefly and the energies of a number of different states based on arrangements or modifications of simple antiferromagnetic linear chains have been estimated. It was found that the total energy was rather insensitive to the details of the local-spin arrangement and it seems clear that the actual

ground state of $Gd(OH)_3$ will be determined by a subtle balance between several relatively small effects. Inasmuch as the interaction Hamiltonian itself is really quite simple and completely known, this should provide an interesting challenge to the theory of cooperative transitions with competing interactions.

ACKNOWLEDGMENTS

We would like to thank S. Mroczkowski and J. Eckert for growing the crystals used in these experiments and C. Sneider for his skillful help in the construction and maintenance of the apparatus. We would also like to thank R. W. Cochrane and C. Y. Wu for helpful discussions and for communicating the results of their work prior to publication.

APPENDIX A

The general expressions for the high-temperature expansions for the susceptibility and specific heat for magnetic systems with arbitrary symmetric tensor interactions between all pairs of spins, have been worked out by Marquard.[47] With the Hamiltonian in Eq. (1), the first coefficients in each expansion are given in Eqs. (4a)–(4c), (14a), and (14b),[101] and we shall here give the explicit expressions for the lattice sums symbolized by the Σ's and the Δ's.

The lattice sums over pairs of spins are

$$\Sigma_{pq}=\sum_j (J_{ij})^p \left(\frac{d}{r_{ij}^3}\right)^q,$$

$$\Sigma'_{pq}=\sum_j (J_{ij})^p \left(\frac{d}{r_{ij}^3}\right)^q \left(\frac{3\cos^2(\theta_{ij})-1}{2}\right),$$

where $d=\frac{1}{2}g^2\mu_B^2$. r_{ij} is the distance between ions i and j and θ_{ij} is the angle between r_{ij} and the c axis. The sums are taken over all distinct pairs of ions i and j with ion i fixed as center and j running over all remaining ions.

Because of the threefold rotational symmetry of the lattice, there is a relation between the sums needed for the susceptibility parallel ($\chi_T^{\parallel}$) and perpendicular ($\chi_T^{\perp}$) to the c axis:

$$(\Sigma_{pq})_\perp=(\Sigma_{pq})_\parallel, \quad (\Sigma'_{pq})_\perp=-\tfrac{1}{2}(\Sigma'_{pq})_\parallel.$$

The double-center sums involving three ions forming triangles are

$$\Delta'_{21}=2\sum_{j>k}\left(J(\vec{r}_1)J(\vec{r}_2)\,\frac{d}{r_3^5}\,\frac{3z_3^2-r_3^2}{2}\right)_{\text{symmetrized}},$$

$$\Delta_{12}=2\sum_{j>k}\left(J(\vec{r}_1)\,\frac{d^2}{(r_2r_3)^3}\,\frac{3\cos^2(\gamma_{23})-1}{2}\right)_{\text{symmetrized}},$$

$$\Delta'_{12}=2\sum_{j>k}\left(J(\vec{r}_1)\,\frac{d^2}{(r_2r_3)^5}\times[\tfrac{3}{4}(3Z^2-R^2)+\tfrac{1}{2}(3z_2^2-r_2^2)r_3^2]\right)_{\text{symmetrized}},$$

where $\vec{R}=\vec{r}_2\times\vec{r}_3$;

$$\Delta_{03}=\frac{1}{6}\sum_{j>k}\frac{d^3}{(r_1r_2r_3)^3}\{9\cos(\gamma_{12})\cos(\gamma_{23})\cos(\gamma_{31}) - 3[\cos^2(\gamma_{12})+\cos^2(\gamma_{23})+\cos^2(\gamma_{31})]+2\},$$

$$\Delta'_{03}=2\sum_{j>k}\frac{d^3}{(r_1r_2r_3)^3}\left(\frac{3\cos^2(\gamma_{12})-1}{2}\,\frac{3Z_3^2-r_3^2}{2r_3^2}\right)_{\text{symmetrized}}$$

We have here introduced $\{\vec{r}_1,\vec{r}_2,\vec{r}_3\}=\{\vec{r}_{ij},\vec{r}_{jk},\vec{r}_{ki}\}$ and γ_{st} as the angle between $\vec{r}_s$ and $\vec{r}_t$. The sums are taken over all distinct triangles with ion i fixed as center and j and k running over all remaining ions. In the symmetrized sums a cyclic permutation of the coordinates is taken and the total divided by three.

As in the case of the Σ's we can relate the coefficients used for the susceptibility parallel and perpendicular to the c axis:

$$(\Delta_{pq})_\perp=(\Delta_{pq})_\parallel, \quad (\Delta'_{pq})_\perp=-\tfrac{1}{2}(\Delta'_{pq})_\parallel.$$

The evaluation of all the lattice sums was performed using the Yale IBM 7040-7094 computer. Special care was taken to avoid double counting or other time consuming steps.[102] All the sums were evaluated within series of spheres of increasing radius R until an adequately accurate extrapolation for the infinite sum could be made. The most slowly convergent was the first-order single dipole sum Σ'_{01}, and this was evaluated for various R's up to 100 Å, corresponding to a sum over 70 000 spins. The sum for an infinite sphere was then estimated as the asymptotic value of the partial sums plotted as a function of $1/R$ as $1/R\to 0$. The estimated accuracy of the extrapolated value was $\pm 0.2\%$. The other single-center sums Σ_{pq} and Σ'_{pq} are more rapidly convergent, and presented no difficulty.

The double-center summations in Δ_{pq} and Δ'_{pq}, on the other hand, were more troublesome, and in particular, the triangular dipole sums Δ_{03} and Δ'_{03} included many small but significant contributions which had to be summed with care. The extrapolation of the partial sums in this case was found to be more rapidly convergent when plotted as a function of $1/N_R$, where N_R is an order of neighbor corresponding to the radius R. This procedure gave Δ_{03} and Δ'_{03} accurate to about $\pm 0.2\%$ for $R_{\max}=20$ Å.

All the computer sums were checked against the published results for $GdCl_3$[47] by substituting the appropriate a and c values and putting $J_3=0$. In all cases agreement was perfect within the estimated accuracies.

Numerical values for the various sums appropriate to $Gd(OH)_3$ were substituted into Eqs. (4a)–(4c), (14a), and (14b), and the final expressions are shown in Eqs. (6a)–(7c), (15a), and (15b).[103]

APPENDIX B: LATTICE SPECIFIC HEATS OF $Gd(OH)_3$ AND $La(OH)_3$

There are two usual methods of estimating the lattice contribution C_L to the total specific heat C_T in calorimetric measurements. One is to measure an isostructural diamagnetic material as similar as possible to the magnetic system and to scale the result by a uniform factor determined either from entropy considerations,[104] or from the ratio of the atomic masses assuming the form of the Debye theory.[105] The second is to assume a specific form for the temperature dependence of C_M and C_L, and then fit the corresponding functions to measurements of C_T on the magnetic material itself. It is of some interest to compare these two procedures in the present case, since the results will illustrate that quite serious errors can occur if great care is not used.

The most common method of analysis is the second, assuming a variation of the form

$$C_T/R = aT^3 + b/T^2, \tag{A1}$$

and using a graphical method one then plots $C_T T^2/R$ as a function of T^5 to look for a straight line of slope a. Such a plot for the case of $Gd(OH)_3$ is shown in Fig. 19 and it can be seen that the results do indeed fall on a fairly good straight line, with $a = (3.4 \pm 0.3) \times 10^{-5}$ K^{-3} and $b = 4.2 \pm 0.4$ K^2. Of course this particular procedure precludes the possibility of determining small higher-order terms in the expansion of C_M [Eq. (13)], and even worse, it is quite sensitive to small deviations from the simple T^3 law, which is really valid only at very low temperatures. In the present case, the Debye temperature $\Theta_D \approx 190 \pm 5$ K,[106] and we would therefore not really expect a simple T^3 law above about 3.5 K ($\simeq \frac{1}{50}\Theta_D$).[105] The fact that the plot in Fig. 19 appears to follow a straight line to much higher temperatures must therefore be treated with some caution. If, as a result of this, we were to concentrate instead on the low-temperature part of the plot, we would run into the difficulty that the higher-order terms in C_M might then not be really negligible, and again an uncertainty in the analysis would result.

To avoid these difficulties, we can consider instead the procedure involving measurements on a similar diamagnetic material, and in Fig. 19 (curve b) we show some results for $La(OH)_3$. For comparison these are plotted in the same way as those for $Gd(OH)_3$, though we would here expect $b \equiv 0$. It can be seen that there is a marked systematic difference, which *cannot* be removed by any simple scaling procedure. In fact scaling the $La(OH)_3$ results by the factor $[M_{La(OH)_3}/M_{Gd(OH)_3}]^{-3/2} = 1.21$ indicated by the Debye theory[105] makes the discrepancy even worse.[107] Moreover, the results

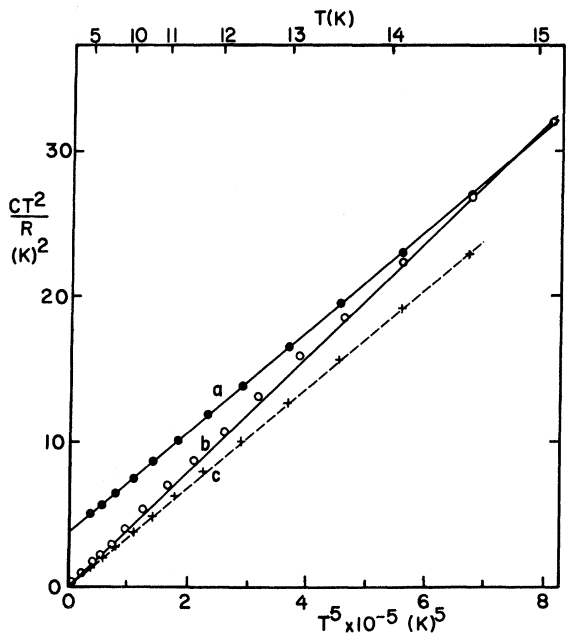

FIG. 19. Calorimetric specific heat of $La(OH)_3$ (o) and $Gd(OH)_3$(•). Curve a is the best fit for $Gd(OH)_3$ assuming a law of the form $C_T/R = aT^3 + b/T^2$ and it corresponds to $a = (3.4 \pm 0.3) \times 10^{-5}$ K^{-3} and $b = 4.2 \pm 0.4$ K^2. The corresponding fit to the results for $La(OH)_3$ (curve b) gives $(a)_{La(OH)_3} = (3.9 \pm 0.3) \times 10^{-5}$ K^{-3}, though it can be seen that there is a systematic curvature which cannot be fitted by the assumed form. Curve c represents the difference between the total specific-heat measurements on $Gd(OH)_3$ and the final estimate of the magnetic contribution based on an analysis of the combined calorimetric and high-frequency measurements (Sec. V A). It corresponds to the "best" estimate of the lattice specific heat $(C_L/R)_{Gd(OH)_3} = (3.4 \pm 0.3) \times 10^{-5}\ T^3$.

are clearly not on a straight line over the entire temperature range, in agreement with our previous fears that a simple T^3 law would be valid only at very low temperatures. We must conclude that the measurements on the diamagnetic isomorph may do no more than give a rough indication of the lattice specific heat of $Gd(OH)_3$ and it raises the more general question of the applicability of this whole procedure.

One should perhaps add another word of caution at this point to note that the kind of comparison shown here is critically dependent on absolute accuracies of two sets of measurements, each of which may involve sizable corrections, and there is always a possibility of undetected systematic errors.

In the present case one can largely resolve these difficulties by combining the calorimetric measurements of C_T with the high-frequency measurements of C_M, which are quite accurate in the region above 5 K (see Sec. V B). Taking the difference, we

find curve c in Fig. 19 which can be approximated quite well by a straight line over the entire temperature range between 5 and 15 K with slope $a = (3.4 \pm 0.3) \times 10^{-5}$ K^{-3}. This is in fairly good agreement with the value found previously and we conclude that $(C_L/R)_{Gd(OH)_3} = (3.4 \pm 0.3) \times 10^{-5} T^3$ which is the value used in the main text.

It would seem clear that the proper allowance for the lattice contribution to the total specific heat is quite a difficult problem, which requires very careful treatment if accurate estimates of C_M are required.

---

†Work supported in part by the U. S. Atomic Energy Commission and in part by the National Science Foundation.

*Present address: RCA Laboratories, Princeton, N.J.

‡Present address: Corning Glass Works, Corning, N.Y.

[1]W. P. Wolf, H. Meissner, and C. A. Catanese, J. Appl. Phys. 39, 1134 (1968).

[2]H. E. Meissner, thesis (Yale University, 1968) (unpublished).

[3]H. E. Meissner and W. P. Wolf, J. Appl. Phys. 40, 1038 (1969).

[4]C. A. Catanese, thesis (Yale University, 1970) (unpublished).

[5]A. T. Skjeltorp and W. P. Wolf, J. Appl. Phys. 42, 1487 (1971).

[6]A. T. Skjeltorp, thesis (Yale University, 1971) (unpublished).

[7]P. D. Scott and W. P. Wolf, J. Appl. Phys. 40, 1031 (1969).

[8]P. D. Scott, H. E. Meissner, and H. M. Crosswhite, Phys. Letters 28A, 489 (1969).

[9]P. D. Scott, thesis (Yale University, 1970) (unpublished).

[10]R. L. Cone and R. Faulhaber, J. Chem. Phys. 55, 5198 (1971).

[11]R. L. Cone, thesis (Yale University, 1971) (unpublished).

[12]R. L. Cone, J. Chem. Phys. 57, 4893 (1972).

[13]R. L. Cone and W. P. Wolf (unpublished).

[14]In a second paper (Ref. 15) we will present magnetothermal measurements and analysis of $Tb(OH)_3$ which is an almost ideal Ising-like ferromagnet.

[15]C. A. Catanese, A. T. Skjeltorp, H. E. Meissner, and W. P. Wolf (unpublished), Paper II in the present series.

[16]P. D. Scott, J. Chem. Phys. 54, 5384 (1971).

[17]R. W. Cochrane, C. Y. Wu, and W. P. Wolf, J. Appl. Phys. 42, 1568 (1971).

[18]R. W. Cochrane, C. Y. Wu, and W. P. Wolf (unpublished).

[19]R. W. Cochrane and W. P. Wolf, Solid State Commun. 9, 1997 (1971).

[20]C. Y. Wu, thesis (Yale University, 1971) (unpublished).

[21]W. P. Wolf, M. J. M. Leask, B. Mangum, and A. F. G. Wyatt, J. Phys. Soc. Japan Suppl. B I 17, 487 (1962).

[22]R. B. Clover and W. P. Wolf, Solid State Commun. 6, 331 (1968).

[23]A. F. G. Wyatt, thesis (Oxford University, 1963) (unpublished).

[24]R. Fricke and A. Seitz, Z. Anorg. Allgem. Chem. 254, 107 (1947).

[25]P. V. Klevtsov and L. P. Sheina, Izv. Akad. Nauk. SSSR., Neorg. Material 1, 912 (1965).

[26]A. N. Christensen, Acta. Chem. Scand. 20, 896 (1966).

[27]A. N. Christensen, R. G. Hazell, and Å. Nilsson, Acta. Chem. Scand. 21, 481 (1967).

[28]There was some question as to whether $Y(OH)_3$ has this symmetry (Ref. 29), but recent results (Ref. 27) show conclusively that $Y(OH)_3$ does have the same structure as the other rare-earth hydroxides.

[29]R. Roy and H. A. McKinstry, Acta. Cryst. 6, 365 (1953).

[30]S. Mroczkowski, J. Eckert, H. Meissner, and J. C. Doran, J. Crystal Growth 7, 333 (1970).

[31]There is general agreement between most of the lattice-constant determinations reported in the literature, with the glaring exception of the early results of Fricke and Seitz (Ref. 24). These older results can therefore be disregarded with some confidence. A good summary of all the lattice constants may be found in Ref. 2. There is some uncertainty in the lattice parameters due to possible variations in stoichiometry, but this effect is expected to be small (<0.1%). Also, since the x-ray studies were made at room temperature, there is an additional uncertainty due to thermal contraction but this is again estimated to be small (<0.1%). The over-all uncertainty in the appropriate lattice constants is therefore estimated to be less than ± 0.3%.

[32]Care was taken to cut each crystal with sharp end faces and, when laid end to end, the air gaps between them were small compared with their diameters. In effect the crystals then appear like one long single crystal.

[33]R. I. Joseph and E. Schlömann, J. Appl. Phys. 36, 1579 (1965).

[34]The demagnetizing factors for ellipsoids are available in literature; see, for example, R. M. Bozorth, *Ferromagnetism* (Van Nostrand, Princeton, N.J., 1964), p. 846.

[35]In other experiments on dry packed powders of hydroxides we found preferential alignments of up to 20% even though care was taken to grind the powder and to avoid any stirring which might induce nonrandomness. This illustrates a problem which may be of importance for preparing "powder" samples of other materials whose typical crystallites are quite aspherical.

[36]R. I. Joseph, J. Appl. Phys. 37, 4639 (1966).

[37]For an extensive list of recent references see Ref. 19.

[38]M. T. Hutchings, R. J. Birgeneau, and W. P. Wolf, Phys. Rev. 168, 1026 (1968).

[39]R. J. Birgeneau, M. T. Hutchings, and W. P. Wolf, Phys. Rev. 179, 275 (1969).

[40]We shall follow the usual custom of expressing all energy parameters in units of K, corresponding to an actual energy k_BK, where k_B is Boltzmann's constant.

[41]R. J. Elliot and K. W. H. Stevens, Proc. Roy. Soc. (London) A219, 387 (1953).

[42]See, for example, M. T. Hutchings, in *Solid State Physics*, edited by F. Seitz and D. Turnbull (Academic,

New York, 1964), Vol. 16, p. 227.

[43]From the ionic radii, we would expect the parameters appropriate to pure $Gd(OH)_3$ to lie between the values corresponding to $Y(OH)_3$ and $Eu(OH)_3$, and probably closer to the latter.

[44]W. Opechowski, Physica 4, 181 (1937).

[45]J. H. Van Vleck, J. Chem. Phys. 5, 320 (1937).

[46]J. M. Daniels, Proc. Phys. Soc. (London) A66, 673 (1953).

[47]C. D. Marquard, Proc. Phys. Soc. (London) 92, 650 (1967).

[48]C. D. Marquard, thesis (Oxford University, 1966) (unpublished).

[49]We prefer this form to the more usual $\chi_T = (\lambda/T) \times (1 + \theta/T + B_2'/T^2 + \cdots)$ since B_2', B_3', etc., are shape dependent, while B_2, B_3, etc., are not.

[50]There is also a small contribution χ_d from diamagnetism. No experimental value for this is available, but it may be estimated to be of order -10^{-6} emu/cm^3 which would be quite negligible.

[51]The partition function can be evaluated treating the Zeeman splitting exactly and the interactions as a perturbation series, using a theory by Van Vleck (Ref. 45) for treating crystal field levels. See also Ref. 52.

[52]W. P. Wolf, B. Schneider, D. P. Landau, and B. E. Keen, Phys. Rev. B 5, 4472 (1972).

[53]W. P. Wolf, J. Phys. (Paris) 32, C1-26 (1971).

[54]J. M. Baker, Rep. Prog. Phys. 34, 109 (1971).

[55]D. P. Landau, B. E. Keen, B. Schneider, and W. P. Wolf, Phys. Rev. B 3, 2310 (1971).

[56]D. P. Landau, thesis (Yale University, 1967) (unpublished).

[57]H. B. G. Casimir and F. K. du Pré, Physica 5, 507 (1938).

[58]C. J. Gorter, *Paramagnetic Relaxation* (Elsevier, New York, 1947).

[59]R. B. Clover and W. P. Wolf, Rev. Sci. Instrum. 41, 617 (1970).

[60]R. B. Clover, thesis (Yale University, 1967) (unpublished).

[61]A. T. Skjeltorp and W. P. Wolf (unpublished).

[62]L. J. F. Broer and C. J. Gorter, Physica 10, 621 (1943).

[63]F. W. DeVrier, J. Volger, and C. J. Gorter, Physica 11, 412 (1946).

[64]Normally, this expression is given in a simplified version assuming $\chi_T(H)/\chi_T(0) = 1$ and $C_M(H, T) = C_M(0, T)$ field independent. See, for example, Ref. 58.

[65]F. R. McKim and W. P. Wolf, J. Sci. Instrum. 34, 64 (1957).

[66]From preliminary measurements (see Ref. 1), a possible cooperative phase transition was erroneously associated with the maximum of the isothermal susceptibility near 2 K.

[67]A. T. Skjeltorp and W. P. Wolf, Am. Inst. Phys. Conf. Proceedings 5, 695 (1972).

[68]M. E. Fisher, Phil. Mag. 7, 1731 (1962).

[69]In contrast to the single-crystal measurements, the powder results have not been corrected to an infinitely long sample shape. Instead, they have been corrected (approximately) to a spherical shape, for which the contribution of long-range dipolar interactions should be least.

[70]The problem of removing the effect of long-range dipolar interactions has been discussed in Ref. 71. In the present case, the approximate mean-field correction is equivalent to a correction to a spherical sample shape.

[71]W. P. Wolf and A. F. G. Wyatt, Phys. Rev. Letters 13, 368 (1964).

[72]It should be noted that the uncertainties in the J's are correlated so that some combinations of J's using the maximum error limits give values for the parameters in Table II outside the quoted errors.

[73]H. A. Buckmaster, Can. J. Phys. 40, 1670 (1962).

[74]D. Smith and J. H. M. Thornley, Proc. Phys. Soc. (London) 89, 779 (1966).

[75]R. J. Birgeneau, Can. J. Phys. 45, 3761 (1967).

[76]The biquadratic exchange is usually characterized by a term of the form $j(\vec{S}_i \cdot \vec{S}_j)^2$ (Ref. 77), but it is really better to use the traceless scaler form $Q\sum_{m=2}^{-2}(-1)^m O_m^2(1) \times O_{-m}^2(2) = Q[\frac{3}{2}(\vec{S}_i \cdot \vec{S}_j)^2 + \frac{3}{4}(\vec{S}_i \cdot \vec{S}_j) - \frac{1}{2}S^2(S+1)^2]$.

[77]P. W. Anderson, in *Solid State Physics*, edited by F. Seitz and D. Turnbull (Academic, New York, 1963), Vol. 14, p. 99.

[78]The lattice spacings increase smoothly from $Y(OH)_3$ to $Eu(OH)_3$, but the changes are quite small, $<0.3\%$ (see Ref. 25). Since the interaction constants seem to vary linearly with ionic separation (see Ref. 19), a good estimate for $Gd(OH)_3$ can therefore be obtained by direct interpolation.

[79]This will be simple, for example, in the case of a ferromagnet, or certain highly anisotropic systems which can be represented by an Ising Hamiltonian.

[80]A well-known example of zero-point motion occurs in the determination of the ground state of Heisenberg antiferromagnets (see, for example, Refs. 81 and 82).

[81]C. Kittel, *Quantum Theory of Solids* (Wiley, New York, 1967), p. 61.

[82]F. Keffer, in *Handbuch der Physik*, edited by H. P. J. Wijn (Springer, Berlin, 1966), Vol. 18, p. 113.

[83]R. J. Birgeneau, R. Dingle, M. T. Hutchings, G. Shirane, and S. L. Holt, Phys. Rev. Letters 26, 718 (1971).

[84]M. E. Lines, Phys. Rev. 164, 736 (1967).

[85]R. J. Birgeneau, J. Skalyo, and G. Shirane, J. Appl. Phys. 41, 1303 (1970).

[86]R. J. Birgeneau, H. J. Guggenheim, and G. Shirane, Phys. Rev. B 1, 2211 (1970).

[87]A. H. Cooke, R. Lazenby, F. R. McKim, J. Owen, and W. P. Wolf, Proc. Roy. Soc. (London) A250, 97 (1959).

[88]M. E. Lines, Phys. Rev. 139, A1304 (1965).

[89]M. E. Lines and E. D. Jones, Phys. Rev. 139, A1313 (1965).

[90]Y. Y. Li, Phys. Rev. 84, 721 (1951).

[91]J. M. Ziman, Proc. Phys. Soc. (London) A66, 89 (1953).

[92]M. E. Lines, Proc. Roy. Soc. (London) A271, 105 (1963).

[93]D. ter Haar and M. E. Lines, Phil. Trans. Roy. Soc. London A255, 1 (1962).

[94]For conciseness we shall express all energies in this section in units of K, suppressing the implied factor k_B/spin. For N spins the energy is then in units of R.

[95]The importance of such small contributions to the energy must not be underestimated, since their effect can be very much enhanced by the stronger *intra*chain interactions. The classic example of this is the two-dimensional square-net Ising model (Ref. 96) with unequal nearest-neighbor interactions, J and J'. For $J' = 0$ the uncoupled linear chains order only at $T = 0$ K, but even a

small $J' \sim 0.01J$ raises the ordering temperature to about 20% of its value for the isotropic case $J = J'$.

[96]L. Onsager, Phys. Rev. 65, 117 (1944).

[97]The error limits given here and for other energies in this section correspond to the maximum ranges allowed by the uncertainties for the J's given in Table III. In comparing energies of different states one must take account of correlations between the different expressions, which will generally tend to reduce the uncertainties in the differences. Also, the relatively large uncertainty quoted for J_3 is probably too pessimistic, since it would seem most probable that J_3 is in fact very close to zero. In making comparisons it is therefore probably best to concentrate on the actual values, even though the quoted ranges of values are allowed by the available parameters.

[98]The summation in this calculation has to be performed with some care since the energies of different sections of the two spirals will vary with the local orientation of the spins (and not only with the *relative* phase angle which remains constant). In practice we took account of this by carrying out an explicit double sum over a large number of spins in both the central spiral (a_n) and the neighboring spirals (b_n, c_n, etc.) for different fixed values of θ. Possible refinements of this procedure are evident, but we shall defer them to a later more detailed study.

[99]See, for example, B. R. Cooper, in *Solid State Physics*, edited by F. Seitz, D. Turnbull, and H. Ehrenreich (Academic, New York, 1968), Vol. 21, p. 393.

[100]T. Nagamiya, K. Yosida, and R. Kudo, Advan. Phys. 4, 1 (1955).

[101]The form of the exchange interactions in the Hamiltonian used by Marquard is $-2\sum_{i>j} J'_{ij}\vec{S}_i \cdot \vec{S}_j$ (Ref. 47). Thus our J_{ij} is equal to $-2J'_{ij}$. This appears as different factors in our expressions for the expansion coefficients compared to those used by Marquard.

[102]A description of the programs used may be obtained from the authors on request.

[103]The numerical values for the individual sums are given in Ref. 6.

[104]J. W. Stout and E. Catalano, J. Chem. Phys. 23, 2013 (1955).

[105]M. Blackman, in *Handbuch der Physik*, edited by S. Flügge (Springer, Berlin, 1955), Vol. 7, p. 325.

[106]Using the relation $C_L/R = 234\ (T/\Theta_D)^3 \simeq 3.4 \times 10^{-5} T^3$.

[107]Comparison of similar estimates of lattice specific heats for other rare-earth hydroxides, (Ref. 4), revealed no systematic trend according to the atomic masses. In fact, it was found that $d[R(OH)_3] \simeq \beta a[La(OH)_3]$ with $\beta = 1.04$, 0.87, 0.97, and 1.07 for R = Nd, Gd, Tb, and Er, respectively.

PHYSICAL REVIEW B VOLUME 7, NUMBER 5 1 MARCH 1973

Third-Order Elastic Constants of $RbMnF_3$ †

E. R. Naimon* and A. V. Granato
Department of Physics and Materials Research Laboratory, University of Illinois, Urbana, Illinois 61801
(Received 3 November 1972)

The complete set of six third-order elastic constants of $RbMnF_3$ has been determined from measurements of hydrostatic-pressure and uniaxial-compression derivatives of natural sound velocities. Measurements were made at room temperature using an ultrasonic pulse-superposition technique. The results are $c_{111} = -18.4$, $c_{112} = -2.4$, $c_{123} = +0.4$, $c_{144} = -0.6$, $c_{155} = -1.8$, and $c_{456} = -0.5$ in units of 10^{12} dyn/cm^2. The results are interpreted to mean that the third-order elastic constants are predominantly determined by the Mn-F interaction. The significance of this for the mechanics of $RbMnF_3$ is discussed.

I. INTRODUCTION

Ultrasonic studies of rubidium manganese trifluoride ($RbMnF_3$) have been reported recently by several authors. Properties studied include second-order elastic constants (SOEC) and their temperature dependence,[1] magnetoelastic coupling,[2,3] nuclear acoustic resonance,[4,5] nuclear magnetic resonance,[6] and ultrasonic attenuation near the Néel temperature.[7,8] Results of the first study of the nonlinear elastic properties of $RbMnF_3$, namely, the third-order elastic constants (TOEC), are reported here.

$RbMnF_3$ belongs to the $Pm3m = O_h^1$ space group and has the familiar perovskite-type cubic crystal structure. All O_h point groups have six independent TOEC.[9] These constants were determined directly from measurements of the hydrostatic-pressure and uniaxial-compression derivatives of natural sound velocities in a single crystal. This is believed to be only the second report of a complete set of TOEC for a perovskite-type crystal structure; TOEC of $SrTiO_3$ were previously obtained by combining the pressure-derivative data of Beattie and Samara[10] with the second-harmonic-generation data of Mackey and Arnold.[11]

II. EXPERIMENTAL PROCEDURE AND RESULTS

A $RbMnF_3$ single crystal was obtained from Isomet Corp., Oakland, N. J., in the shape of a 1-cm cube. Faces of the cube were near {001}, {110}, and {1$\bar{1}$0} planes; misorientations of the respective